The Effects of D-galactose Administration on Senescence and Atrial Fibrillation Induction in Rats

Allan Ochs

Department of Pharmacology and Therapeutics

McGill University

Montréal, Quebec, Canada

January 2025

A thesis submitted to McGill University

in partial fulfillment of the requirements of the degree of

Master of Science

ABSTRACT

Cellular senescence refers to a process producing cell cycle arrest that can result from a plethora of cellular stresses. Senescent cells are characterized by their proinflammatory and prothrombotic profile, as well as their inability to proliferate even in the presence of mitogenic factors. They can, however, influence neighbouring cells through what is collectively referred to as the senescence-associated secretory phenotype (SASP) characterized by the secretion of specific cytokines, chemokines, proteases, growth factors, and lipids. Transient presence of senescent cells in the heart may prove beneficial, whereas long-term accumulation impairs cardiac function and promotes age-related decline. While classically described in multiplying cell-types, similar biochemical processes can occur in terminally-differentiated cells like cardiomyocytes. The prevalence of atrial fibrillation (AF), the most common sustained cardiac arrhythmia, increases with age and affects nearly one million Canadians, most of whom are seniors. AF and the role aging plays in its development are both poorly understood, and current therapies are inadequate at addressing the aging substrate of AF. Given the notable increase in morbidity and mortality in elderly patients with AF, the need for an accelerated aging model with which to study aging as a substrate for AF is clear. Administration of D-galactose is a widely used model for senescence. D-galactose is thought to generate reactive oxygen species via its metabolism to cause cellular damage and has shown promise as a means of replicating senescent-associated arrhythmias. To develop a model to study the role of cardiac senescence resulting in AF, eight-week-old male and female Sprague Dawley rats were injected daily with various doses (150, 300, and 500 mg/kg) of D-galactose in saline solution for eight weeks. Structural heart parameters were

collected both before and after the study using echocardiographic imaging. At the end of eight weeks, electrophysiology (EP) parameters and AF inducibility were assessed through intracardiac measurements. After EP study, the hearts were excised and assessed for either SASP marker gene expression through qPCR, or for fibrosis using Masson Trichrome staining. Adequate D-galactose absorption into the systemic circulation was confirmed using a colorimetric detection assay. Our results indicate that D-galactose dosed rats displayed no significant differences in gene expression, nor did they exhibit AF inducibility, increased collagen deposition, or structural parameter changes when compared to their controls.

The D-galactose induced senescence model seems unable to replicate the electrophysiological changes observed in natural aging and cannot be used to reliably study the effect of aging on the development of AF. Further exploration is needed to evaluate whether this model can reliably induce a senescent or an aging-like phenotype.

RESUME

La sénescence cellulaire fait référence à un processus produisant un arrêt du cycle cellulaire qui peut résulter d'une pléthore de stress cellulaires. Les cellules sénescentes se caractérisent par leur profil pro-inflammatoire et prothrombotique, ainsi que par leur incapacité à proliférer même en présence de facteurs mitogènes. Elles peuvent cependant influencer les cellules voisines par le biais de ce que l'on appelle collectivement le phénotype sécrétoire associé à la sénescence (SASP), caractérisé par la sécrétion de cytokines, chimiokines, protéases, facteurs de croissance et lipides spécifiques. La présence transitoire de cellules sénescentes dans le cœur peut s'avérer bénéfique, alors que l'accumulation à long terme altère la fonction cardiaque et favorise le déclin lié à l'âge. Bien que classiquement décrits dans les types de cellules en multiplication, des processus biochimiques similaires peuvent se produire dans les cellules à différenciation terminale comme les cardiomyocytes. La prévalence de la fibrillation auriculaire (FA), l'arythmie cardiaque soutenue la plus courante, augmente avec l'âge et touche près d'un million de Canadiens, dont la plupart sont des personnes âgées. La FA et le rôle que joue le vieillissement dans son développement sont tous deux mal compris, et les thérapies actuelles sont inadéquates pour traiter le substrat vieillissant de la FA. Compte tenu de l'augmentation notable de la morbidité et de la mortalité chez les patients âgés atteints de FA, la nécessité d'un modèle de vieillissement accéléré permettant d'étudier le vieillissement en tant que substrat de la FA est évidente. L'administration de D-galactose est un modèle de sénescence largement utilisé. Le D-galactose est soupçonné de générer des espèces réactives de l'oxygène par le biais de son métabolisme pour causer des dommages

cellulaires et son administration s'est avérée prometteur comme moyen de reproduire les arythmies associées à la sénescence. Afin de développer un modèle permettant d'étudier le rôle de la sénescence cardiaque dans la FA, des rats Sprague Dawley mâles et femelles âgés de huit semaines ont reçu une injection quotidienne de différentes doses (150, 300 et 500 mg/kg) de D-galactose dans une solution saline pendant huit semaines. Les paramètres cardiaques structurels ont été recueillis avant et après l'étude par échocardiographie. Au bout de huit semaines, les paramètres électrophysiologiques (EP) et l'inductibilité de la FA ont été évalués par des mesures intracardiaques. Après l'étude EP, les cœurs ont été excisés et évalués pour l'expression de gènes associés au SASP par qPCR, ou pour la fibrose par coloration au trichrome de Masson. L'absorption adéquate du D-galactose dans la circulation systémique a été confirmée à l'aide d'un test de détection colorimétrique. Nos résultats indiquent que les rats traités au D-galactose ne présentent pas de différences significatives dans l'expression des gènes, ni d'induction de la FA, ni d'augmentation du dépôt de collagène, ni de modifications des paramètres structurels par rapport à leurs témoins.

Le modèle de sénescence induite par le D-galactose semble incapable de reproduire les changements électrophysiologiques observés lors du vieillissement naturel et ne peut être utilisé pour étudier de manière fiable l'effet du vieillissement sur le développement de la FA. D'autres études sont nécessaires pour déterminer si ce modèle peut induire de manière fiable un phénotype de sénescence ou de vieillissement.

AUTHOR CONTRIBUTIONS

Allan Ochs – Performed animal experiments (D-galactose preparation and administration, tissue and blood sampling, echocardiographic analysis, and electrophysiological analysis), RNA extraction and RT-qPCR analysis, histological analysis, D-galactose quantification ELISA, statistical analysis, and thesis writing.

Édouard Marcoux – Aided with electrophysiology studies and performed the associated surgeries.

Patrice Naud – assisted with RT-qPCR and ELISA experiments and provided instruction on experimental operations.

Jean-Claude Tardif - supervised experiments and blind analyses of echocardiography.

Martin G. Sirois and Jean François Tanguay - co-supervised experiments and blind analyses for histological experiments.

Stanley Nattel - contributed to the initial concept of the study, assisted with project development and supervision, and provided intellectual and editorial input.

ACKNOWLEDGEMENTS

ישמחו השמים ותגל הארץ

First and foremost, I proclaim thanks to my God, the God of my forebearers, who gives me the opportunity to study and learn and who has brought me to this point.

I would like to express heartfelt gratitude to Dr. Stanley Nattel for providing me with both the space and opportunity to develop as a budding scientist. Your tutelage and expertise as well as your passion for and dedication to science have served as both a resource and a motivation for my growth these past few years.

I would also like to both thank and acknowledge the support and guidance of my supervision committee members: Dr. Bruce Allen and Dr. Éric Thorin. Your insight and probing questions always stuck with me in our discussions and were invaluable in directing my research and exploration.

I also would like to extend immense thanks to my advisor Dr. Terry Hebert for his unwavering support throughout my degree and his situational wisdom, realism, and guidance. I cannot thank you enough for the security of knowing you were looking out for me.

To all the committed members of the Nattel lab, it has been a pleasure to work with and alongside you. Thank you for the support and collaboration. I consider every moment of our interaction integral to the development of my scientific journey. Many thanks specifically to Dr. Patrice Naud and Dr. Xiaoyan Qi for teaching me various lab techniques and their ongoing help and support. In addition, thank you to Chantal St-Cyr for organizational help,

communication assistance, and for always reinforcing my self-advocacy skills. Thank you to Jennifer Bacci for secretarial help and for our many amazing conversations.

Thank you to the amazing animal facility team at the MHI and especially to Marie-Ève Higgins and Samantha Zicari for amazing technical assistance. I would not have been able to perform all my experiments without you.

To Dr. Anna Garcia-Elias, thank you for warmly welcoming me to both the lab and scientific research. Your constant guidance and care were the impetus for my undertaking of scientific research.

To Dr. Mozhdeh Mehdizadeh, thank you for looking out for me and taking me under your wing. Including me in your work was always educational and made me feel looked after within the lab. I'm so happy we were able to work together, and I appreciate our friendship that has grown out of it.

I would especially like to thank my chosen family at the lab, Édouard Marcoux and Deanna Sosnowski, for their constant support and unwavering friendship both in the lab and in life. I hope that the strength of our shared bonds continues as Ecclesiastes notes, "A threefold cord is not readily broken."

To Dr. Svenja Koslowski, Thank you for your companionship and care throughout this past year. I have been so honoured to receive your kindness and compassion in more ways than I can recount. Your attention to all things important has preserved my health and sanity in critical periods, and I look forward to continuing our friendship.

Thank you to my aunt Ruth Nadler for support and aid over the course of my studies. You've bailed me out many times and in many ways. I love you and cannot thank you enough.

Thank you to my parents, my extended family, my many friends, and the community of Chabad McGill who each helped me along in their own way.

This thesis is dedicated to all of you. Know that without each of you, there is no way this thesis would have come to be.

TABLE OF CONTENTS

TABLE OF FIGURES

TABLE OF TABLES

LIST OF ABBREVIATIONS

AERP	Atrial effective refractory period
AF	Atrial fibrillation
AGE	Advanced glycation end products
ANOVA	Analysis of variance
AP	Action potential
CL	Cycle length
cSNRT	Corrected sinus node recovery time
ECG	Electrocardiogram
ECM	Extra-cellular Matrix
EDT	E-wave deceleration time
EF	Ejection fraction
ELISA	Enzyme linked immunosorbent assay
ERP	Estimated refractory period
FS	Fractional shortening
LA	Left atrial
LV	Left ventricular
LVEF	Left ventricular ejection fraction

LVFS	Left ventricular fractional shortening
MCT	Multiple comparisons test
MMP	matrix metalloproteinase
PBS	Phosphate buffered saline
PCR	Polymerase chain reaction
qPCR	Quantitative PCR
RAGE	Receptor for AGEs
RB	Retinoblastoma
ROS	Reactive oxygen species
SASP	Senescence-associated secretory phenotype
SEM	Standard error of the mean
SNRT	Sinus node recovery time
WBP	Wenckebach point
WT	Wild-type

1 INTRODUCTION

1.1 The heart and its rhythm

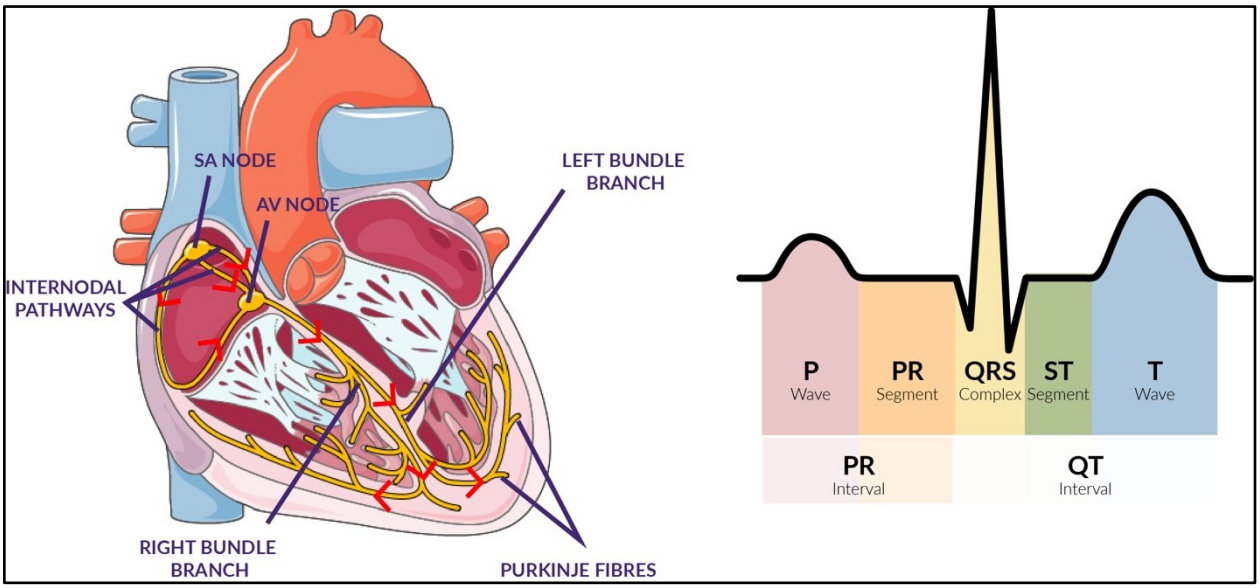

Figure 1. Overview of the heart's conduction system and electrical waveform depiction. *Adapted from Cardarilli et al. (2019)[1] using Servier Medical Art and adapted for clarity. Licensed under CC BY 4.0 (https://creativecommons.org/licenses/by/4.0/)*

A functioning heart pumps blood through the body by contracting its muscles, varying its rhythm to accommodate physiological needs.[2] The pulse of the rhythm as contraction spreads across the tissue reflects the interplay in propagation of electrical activity both between and within cardiac myocytes.[3,4] Within cardiac myocytes, electrical activity during contraction and relaxation is observed as changes in the cardiomyocyte membrane potential and the resultant waveform is referred to as the cardiac action potential (AP). When observed at the tissue level, cardiac APs generate macroscopic electrical activity over time, summated in the electrocardiogram (ECG), which depicts the propagation of electrical activity through the tissue for a single unit of the cardiac cycle or a heartbeat (**Figure 1**).[4] The ECG depicts distinct waveforms corresponding to the membrane polarization changes over

the cardiac cycle. The cardiac cycle begins at the sinoatrial node with spontaneously and automatically generated APs and propagates across both atria. It then passes through the atrioventricular node, down the His-Purkinje system and through the ventricles and elapses enough time to allow for repolarization before beginning anew. Correspondingly, the ECG depicts the P-wave for atrial depolarization, the QRS complex for ventricular depolarization, and the T-wave for ventricular repolarization (**Figure 1**).[5]

1.2 Atrial fibrillation

Atrial fibrillation (AF) is the most prevalent sustained cardiac arrhythmia clinically. It is associated with a decreased quality of life and an increase to morbidity and mortality.[6,7] Risk factors that are associated with AF development can be classified into two groups – modifiable and unmodifiable. Modifiable risks include obesity, substance use such as tobacco and alcohol, sleep apnœa, and physical inactivity. It also includes conditions that respond to treatment, such as type II diabetes mellitus, high blood pressure, and even heart failure. Genetic background, race, ethnicity, and sex are examples of some unmodifiable risks that contribute to the likelihood of developing AF. Aging is a factor of AF development that is crucial to study, precisely because it is both unmodifiable and universal.[8–10] The prevalence of AF is shown to increase with age – from approximately two percent of the general population to over 10 percent when looking at octogenarians. As the elderly segment of the population grows the burden of AF increases in tandem and can place further strain on a beleaguered healthcare system to the tune of hundreds of millions of dollars.[11,12] AF is characterized by the loss of sole control by the sinus node pacemaker over the heart's contraction and exhibits rapid and irregular activation of the atrium. It leads to a defect in

the efficiency of the heart's ability to adequately pump blood and causes a significant increase in the likelihood of occurrence for both strokes and heart failures. AF is classified based on its persistence: paroxysmal for events that terminate within seven days, persistent for less than a year, longstanding persistent for greater duration where treatment is pursued, and permanent.[7,11,13]

1.2.1 Atrial remodelling

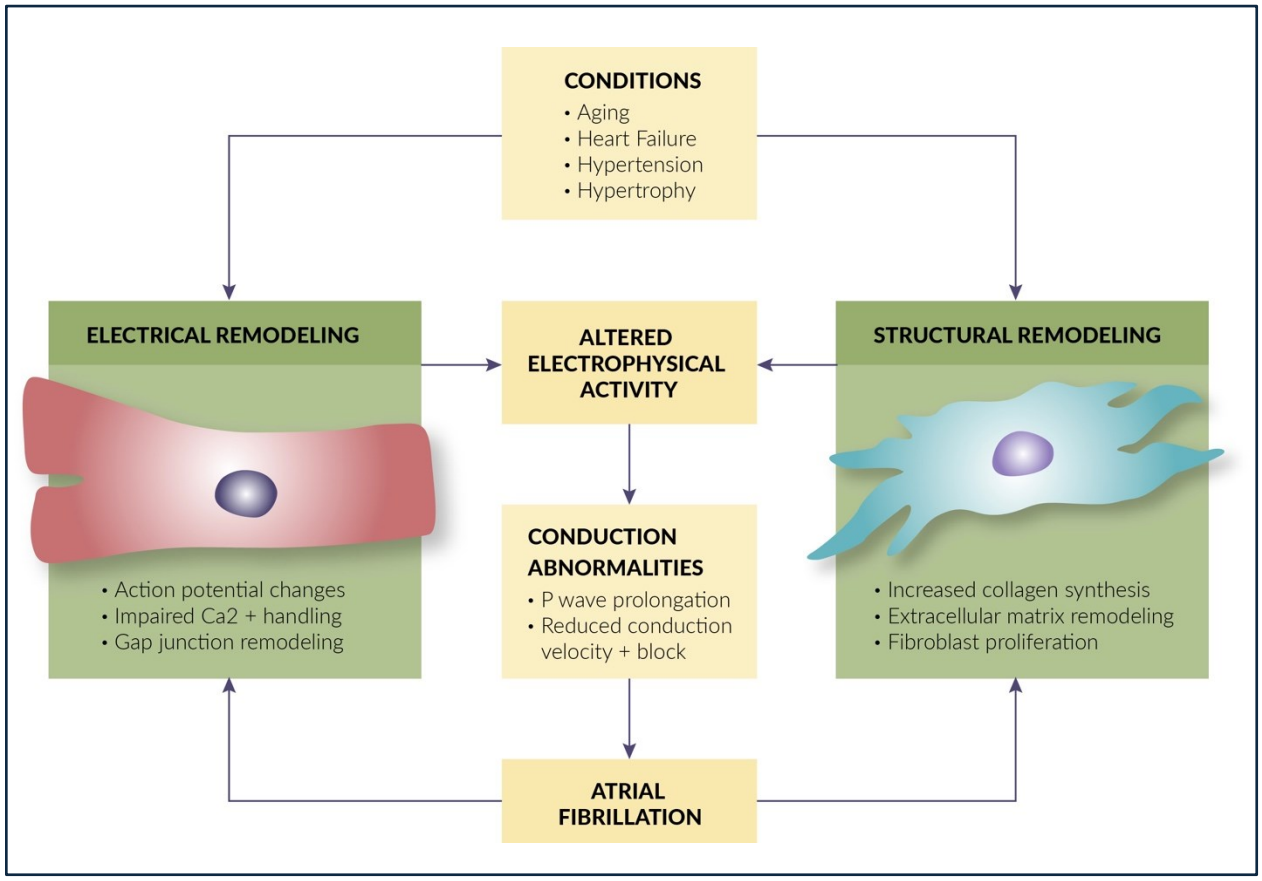

Figure 2. Overview of atrial remodelling. *Adapted from Jansen et al. (2020)*[14]

Atrial remodelling, initially from underlying conditions and subsequently from the AF itself, drives the progression of AF from paroxysmal to permanent (**Figure 2**).[15] Atrial remodelling describes the time dependent adaptation of the atrial tissue and its composite cell

populations in response to stressors in an attempt to maintain homeostasis.[16] Remodelling alters the electrical and structural properties of the atrial tissue. Atrial tissue refractory periods are shortened during AF and corrected sinus node recovery time (cSNRT) is lengthened and can serve as a hallmark of risk of AF recurrence and worsening.[17,18] Altered heart rates being either too fast or too slow, as well as changes to the duration of heartbeat subparts – such as the QRS complex duration – as a function of remodelling, are also associated with AF progression and recurrence.[19–21] As AF persists towards permanent, structural tissue changes play a role in effecting lasting and irreversible AF. Persistence of AF is shown to result in enlarged atria and can subsequently lead to ventricular dysfunction.[22,23] It also increases myocardial fibrosis by increasing collagen deposition making conductive tissue more heterogenous. The enlargement of tissue area and increased insulative properties of fibrosis further compound with the remodeled electrical properties, such as shortened refractory times driving AF towards permanence.[24,25] Notably, aging also drives remodelling as the atria naturally dilates with increased age and myocardial fibrosis increases generating conditions susceptible to AF onset.[23,26] Thus, understanding the mechanisms of aging becomes imperative in the greater context of AF development and progression.

1.3 Senescence: aging as a pathology

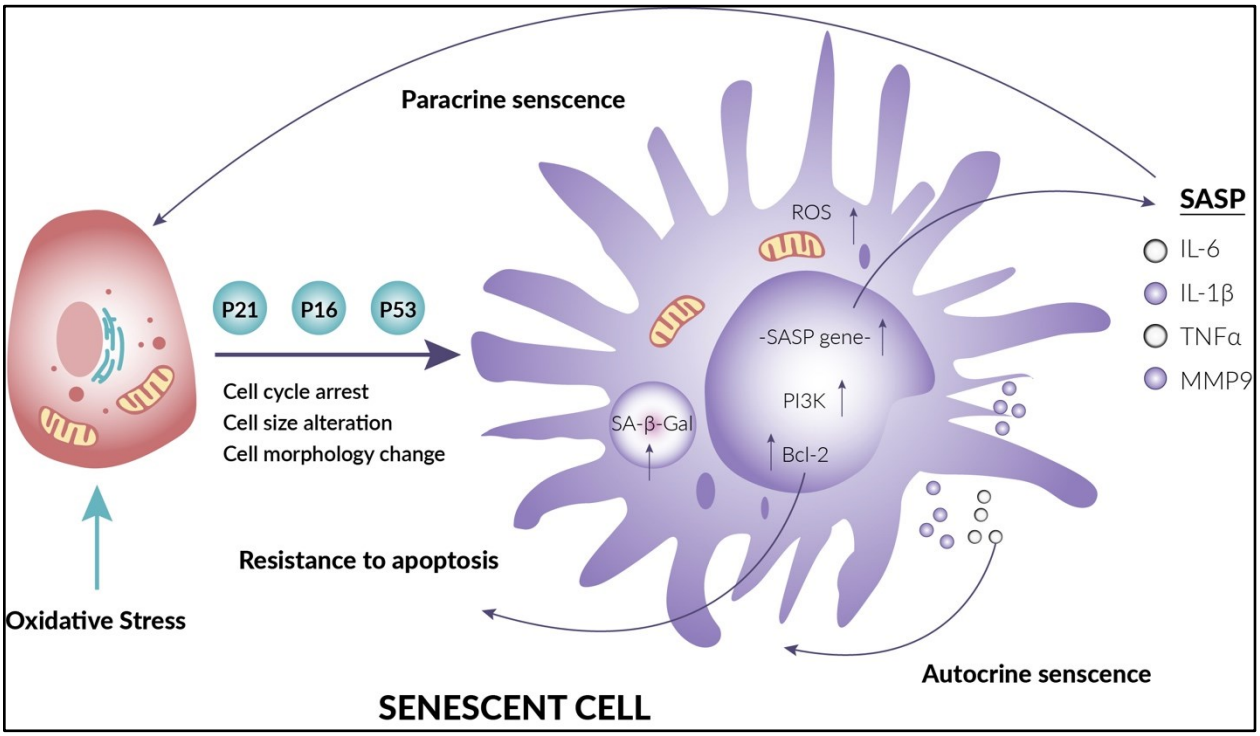

Figure 3. Simplified overview of senescence. *Adapted from Xiao et al. (2023)*[27]

Senescence describes a cellular process that limits the proliferation of aged or damaged cells. Senescent cells are often found in conjunction with tumors and aged tissue.[28,29] Pathologically, it is linked to two main pathways: p53/p21 and p16/retinoblastoma (RB). Senescent interference in these pathways inhibit cyclin-dependent kinases necessary for the phosphorylation of crucial transcription factors involved in genes related to G1 to S phase transition in the cell cycle.[30–32] Senescent cells impact their environs through the paracrine release of lipids, proteases, and inflammatory chemokines and cytokines collectively called the senescence-associated secretory phenotype (SASP) (**Figure 3**).[33] These secretions in turn can dually propagate senescence to healthy cells in the surrounding environment, while also reinforcing the senescent response of the secreting cell in an

autocrine manner. Furthermore, the SASP also can generate local inflammatory responses and subsequent tissue damage and remodelling.[28]

1.3.1 Senescence in the heart

Senescence affects cell function differently depending on the cell type and location.[34] Although senescence is generally associated with replication, post-mitotic cells like cardiomyocytes can still become senescent and can modify surrounding cells via their inflammatory and extracellular matrix (ECM) modifying SASP components.[35] They also display the hallmark upregulation of *p16*, *p21*, and *p53* found in senescent mitotic cells.[36] Notably, there are also populations of mitotic cells within the heart that contribute to overall aging and localised senescence. Endothelial and epithelial cells, fibroblasts, and immune cells all experience cell-cycle arrest when senescent and present upregulated expression of *p16*, *p21*, and *p53* as well as inflammatory and ECM-remodelling SASP components such as *Il-6*, *Tnfα*, matrix metalloproteases (MMPs), and *Tgfβ2*.[36,37] The interplay of senescence and SASP between the various cell populations of the heart can initiate major adverse consequences such as fibroblast activation and cardiomyocyte hypertrophy and even cell death.[38]

1.3.2 Inflammaging

Inflammaging while distinct in concept is linked to senescence. It refers to chronic low-grade inflammation developed with age and plays a role in cardiac disease.[39] Sustained inflammation, in contrast to inflammation as a defense against infection, can be detrimental to health.[40] In the heart, constant inflammation is linked to mitochondrial damage and

reactive oxygen species (ROS) production both of which are also linked to cellular senescence.[41,42] Systemically, it is characterized by upregulation of proinflammatory markers similarly upregulated in senescent cells and SASP production such as *Il-6*, *Tgfβ* and *Tnf*.[39] Given the interplay between physiological changes of senescence, inflammation, aging, and remodelling, it is imperative to study and understand the roles played by these changes in the development of AF.

1.4 D-galactose administration: a model for accelerated aging and senescence

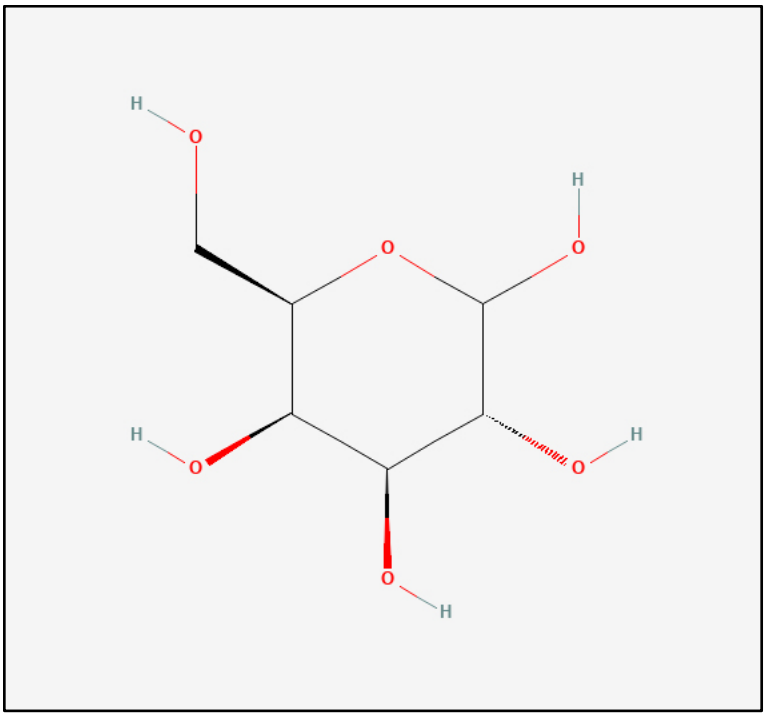

Figure 4. 2-D structure of D-galactose. *National Center for Biotechnology Information. PubChem Compound Summary for CID 6036, D-Galactose. https://pubchem.ncbi.nlm.nih.gov/compound/D-Galactose. Accessed Nov. 5, 2024.*

D-galactose (**Figure 4**) is a hexose sugar critical for human metabolism and development. It is an epimer of glucose at the fourth carbon and cannot be metabolized as is. In physiological conditions D-galactose favours a β-oriented anomeric carbon and must be

enzymatically mutarotated to an α-oriented anomer and epimerized to glucose to undergo glycolysis in a process known as the Leloir pathway.[43,44] The energy cost of the process results in metabolic energy being derived from mitochondrial oxidative phosphorylation which can result in ROS damage to tissue.[45,46] Another important metabolic pathway of D-galactose involves oxidation catalyzed by galactose dehydrogenase, producing a metabolite called galactonate which is either excreted in urine or funneled into the pentose phosphate pathway and can protect against oxidative stress.[47,48] Excessive accumulation of D-galactose is addressed physiologically in three routes that form the underpinning of the induced aging and senescence model, all of which result in excessive ROS and oxidative stress (**Figure 5**):

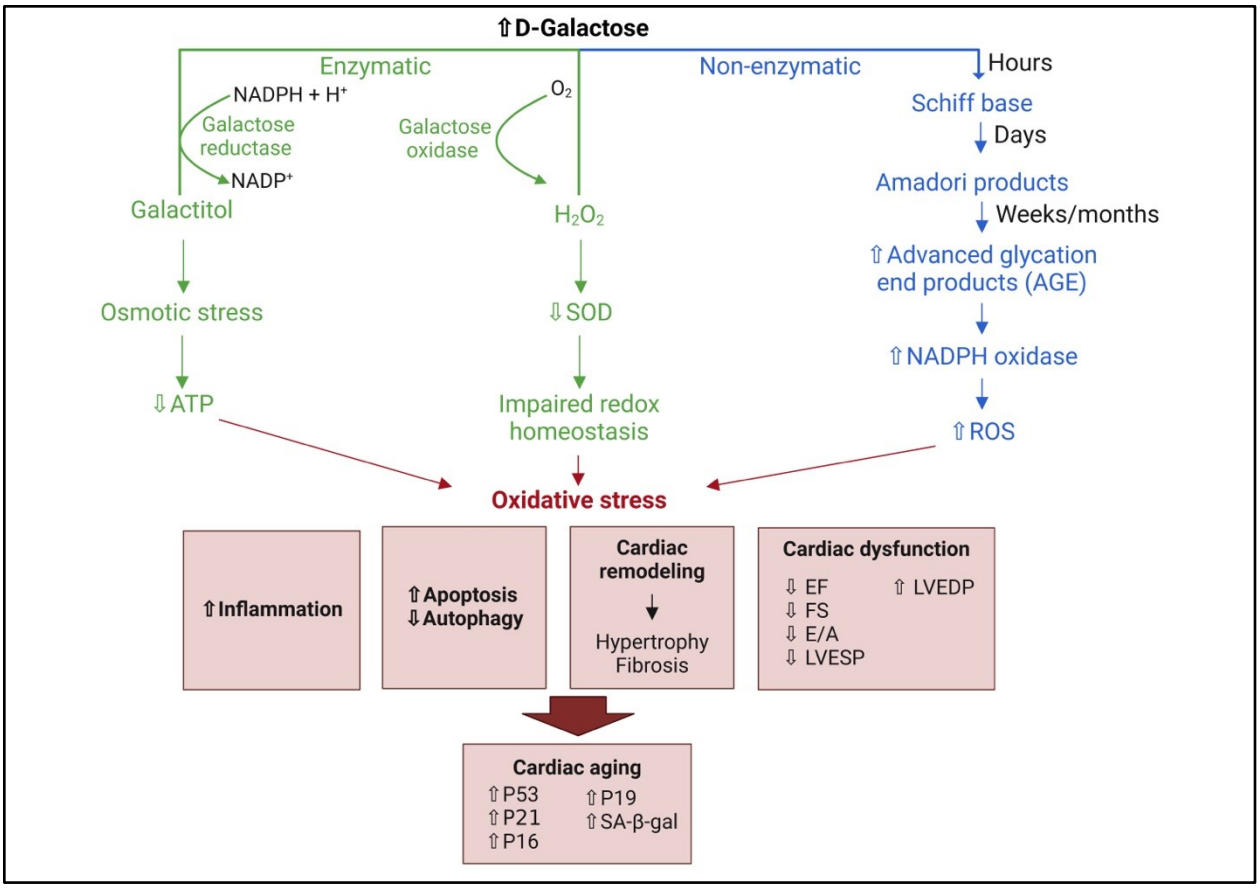

Figure 5. D-galactose administration model reported mechanistic overview. *Adapted from Bo-Htay et al, (2018)[49], Azman and Zakaria (2019)[50] and Wang et al. (2022)[51]*

1.4.1 Metabolism of excess D-galactose

1.4.1.1 Enzymatic pathways

Beyond the Leloir and pentose phosphate pathways, two enzymes are reported to metabolize excess D-galactose. Galactose reductase, also referred to as aldose reductase, reduces galactose to the polyalcohol galactitol which is a product that cannot be further metabolized and due to poor diffusion also accumulates in cells and exerts osmotic stress resulting in mitochondrial dysfunction.[48–50] As well, galactose oxidase will yield a hexadialdose and hydrogen peroxide as a byproduct leading to reduced levels of superoxide dismutase and impaired redox homeostasis.[49,50] Both of these auxiliary metabolic pathways

produce ROS and lead to inflammation, degeneration, and apoptosis, similar to conditions in aging and related disorders.[50]

1.4.1.2 Non-enzymatic processing of D-galactose

Aldose sugars at elevated concentrations, in persistent contact with amines and lipids, and in environments of oxidative stress will form advanced glycation end products (AGE) via the Maillard reaction. The resultant permanent cross linking of proteins decreases solubility and can increase organ stiffness and fibrosis. Furthermore, AGEs interact with specialized receptors to increase hypertrophy, inflammation, fibrosis, and cell cycle arrest. It also triggers an increase in the presence of NADPH oxidase and results in greater oxidative stress.[50,52,53] Given how AGEs result from and produce oxidative stress and how imbalanced redox homeostasis additionally impacts oxidative stress in the enzymatic pathways of the accelerated aging model, it is important to see the model as not just three distinct pathways, but as degenerative routes that feed and cycle into one another.[49,50]

1.4.2 D-galactose model history and application

The D-galactose administration model emerged in the latter half of the 1980s, initially for the study of the development of cataracts. It was noted that rats fed with a large fraction of their diet being D-galactose had a significantly larger propensity to develop cataracts than those fed regular chow due to the increased osmotic stress.[54–56] By the start of the 1990s, D-galactose administration was employed by researchers and reported in Chinese and subsequently international journals to track toxic effects of D-galactose and mimic aging outcomes.[57] While the initial studies performed by Zhang et al. (1990, 1996) were not

accessible due to language and access barriers, they have been cited extensively in subsequent publications.[50,58,59] Within a decade of its adoption as an accelerated aging model, D-galactose administration began to be used to induce cellular senescence.[60] Over time, the D-galactose administration model expanded from testing the effectivity of natural remedies and Chinese medicine, to evaluating pharmacological compounds, generating disease states for the study of conditions such as diabetes and renal amyloidosis, and therapeutic interventions.

1.4.3 Relevant findings of the effect of D-galactose administration on cardiac outcomes

D-galactose administration in cardiac aging and senescence studies yields promising results for further use (**Table 1**). Classical markers of senescence like *p53* and *p21* are shown to be upregulated in dosages as low as 100mg/kg/day and for treatment durations of as little as 6 weeks.[61,62] Some studies also noted D-galactose administration led to the upregulation of inflammatory and ECM-modulating SASP markers such as *Il-6*, *Tnfα*, and *Mmp9* in low-dose regimens in both mice and rats.[63–65] Furthermore, oxidative stress and damage was consistently observed with D-galactose administration over both sexes even with larger species such as dogs.[66–68] Various studies have also reported an increased presence of AGEs and increased expression of receptor for AGEs (RAGE) as a result of D-galactose.[64,69,70] Beyond markers of inflammation noted in SASP upregulation, reported signs of induced cardiac aging in D-galactose administered include reduced left ventricular ejection fraction (LVEF) and fractional shortening (FS), cardiac hypertrophy, and increased collagen deposition and fibrosis.[71–73] Echocardiographic changes included increased heart rates, PR

intervals, and QRS intervals.[74] Some studies reported that D-galactose was able to induce myocardial injury, and only one study was able to induce AF.[63,75]

1.5 Aim

In light of the background information above, our goal was to extend and standardize the D-galactose administration model such that it could be reliably used to study the effects of aging on the heart to better understand AF development.

Table 1. *Overview of most relevant literature on D-galactose administration focused on cardiac outcomes*

Author	Animal (Sex)	Sex	Age at Start (weeks)	Duration (weeks)	Dosage (mg/kg/day)	Route	Relevant Findings
Cebe et al., 2014[76]	Rat/ Wistar (Male)	M	22	6	60	IP	No significant differences observed between model and naturally aged groups at all. No comments relate to differences to young controls
Wang et al., 2018[61]	Mouse/ NOT SPECIFIED	N/A	NOT SPECIFIED	6	100	SC	Upregulated expression of p53, p21, caspase 1, IL-1β
Chang et al., 2021[77]	Rat/ Wistar-Kyoto (Male)	M	20	8	150	IP	EF% & FS% Significantly reduced ($p<0.1$) p21, βgal, cycD1 expression significantly increased ($p<0.001$) Bcl-2 expression decreased ($p<0.01$)
Bo-Htay et al., 2020[78]	Rat/ Wistar (Male)	M	200-220 (g)	4 and 8	150	SC	FS% significantly reduced; BP significantly increased (cleaved casp-3/casp-3) expression increased, Tunnel Positive cells percentage significantly increased
Feng et al., 2021[79]	Mouse/ C57BL/J6 (Male)	M	8	8	200	SC	Significant decrease in EF% and FS%, levels of ANP and BNP were significantly increased, increased oxidative stress status

Chang et al., 2018[65]	Rat/ Sprague-Dawley (Male)	M	8	8	150	ROUTE NOT SPECIFIED	Up-regulated TGFβ1, p-MEK1/2, and p-ERK1/2, SP1 & CTGF increased, FGF2, uPA, and MMP9 protein levels increased
Guo et al., 2017[80]	Rat/ Sprague-Dawley (Male)	M	13	6	125	SC	Bcl-2 reduced protein expression significantly reduced
Chang et al., 2016[81]	Rat/ Sprague-Dawley (Male)	M	8	8	150	IP	Tunnel positive cell percentage significantly increased $p<0.001$, Fas/FADD/Caspase-8 upregulated
Ge et al., 2021[82]	Mouse/ SPF Kunming (Male)	M	8 to 9	4	500	SC	Significantly lower bodyweight, Increase in Oxidative stress
Ma et al., 2021[75]	Mouse/ Kunming (Male)	M	6 to 8	9	500	IH	Induced myocardial injury. Increased p21 expression/βgal positive cells/ ROS level in myocardium
Li et al., 2021[83]	Rat/ Sprague-Dawley (Male)	M	200-230 (g)	8	200	IP	Decline in BW, organ-indices suggest atrophy and decreased SOD levels
Zhang et al., 2022[63]	Rat/ Sprague-Dawley (Male)	M	6 to 8	6	125	SC	Induced AF, Bodyweight decrease, Increase in p53/p21 expression, plasma levels of pro-inflammatory cytokines TNF-α, IL-1βand IL-6 were significantly higher the anti-

							inflammatory cytokine IL-10 was lower in aging group
Maharajan and Cho, 2021[64]	Mouse/ C57BL/J6 (Male)	M	6	10	150	IP	Catalase and p53/p21 expression increased, oxidative stress increased, (RAGE) and the levels of inflammation markers (IL1α, IL1β, and IL6) enhanced.
Hong et al., 2021[72]	Mouse/ C57BL/J6 (Male)	M	8 to 10	10	150	SC	EF%/FS% statistically reduced, Increased p53/p21 relative to GAPDH, PINK1/Parkin/Sirt6 reduced relative to GAPDH
Charriere et al., 2016[84]	Human (Male)	M				PO	HR and stroke volume changes though muted in D-Galactose group
Strother et al., 2001[85]	Rat/ Sprague-Dawley (Male)	M	175-200 (g) + 1 week acclimation	4	50% of Diet	PO	BW significantly reduced,
Ji et al., 2017[66]	Dog/ Beagle (Mixed)	X	104	13	50	SC	MDA increased. SOD decreased. Increased protein expression of p16 and p21 relative to GAPDH

Lin et al., 2020[71]	Rat/ Wistar-Kyoto (Male)	M	18	4	150	null	Rac-1, Nox-2 upregulated, Nrf2 HO-1, SOD-1 downregulated, IkB expression reduced, cardiac hypertrophy, collagen deposition in induced aging group
Zhu et al., 2019[86]	Mouse/ ICR (Mixed)	X	6	6	120	IP	Oxidation increased in D-Gal group, not much by way of heart besides organ index
Xue, Aliabadi & Hallfrisch, 2001[87]	Rat/ Sprague-Dawley (Male)	M	weanling 50-60 (g)	36 and 88	50% of Diet	PO	Galactose fed rats had retarded growth compared to other diets. Individual organ indices however were increased
Chen et al., 2018[88]	Rat/ Sprague-Dawley (Male)	M	13	8	150	IP	TNF-α, TNF-R, p-NFκB, COX2 increased relative to α-tubulin
Lay et al., 2020[89]	Rat/ Sprague-Dawley (Male)	M	4	8	150	IP	Tunnel positive cells 6.5x higher, larger amount of collagen accumulation, Fas/Caspase-8 upregulated relative to α-tubulin, Bax/cleaved casp-3/cleaved PARP relative to β-actin
Yager et al., 2003[90]	Mouse/ GALT Deficient (mixed)	X	3	NOT SPECIFIED probably 4 weeks	40% of Diet	PO	Galactitol accumulation highest in heart
Zhang et al., 2021[91]	Mouse/ C57BL/J6 (Male)	M	8	13	125	SC	EF%/FS% daily variation disrupted and reduced in induced aging model

Bo-Htay et al., 2020[78]	Rat/ Wistar (Male)	M	NOT SPECIFIED	8	150	SC	Decrease in LVEF in D-Gal treated group
Park et al., 2020[92]	Mouse/ C57BL/J6 (Male)	M	12	12	500	SC	D-Gal administration alone does not induce hearing loss or aging-like phenotype
Qian et al., 2018[93]	Mouse/ Kunming (Mixed)	X	6	6	120	IP	Decreased organ indices including heart
Li et al., 2019[94]	Mouse/ Kunming (Male)	M	6	8	120	PO?	Decreased organ indices including heart,
Maharajan et al., 2021[69]	Mouse/ C57BL/J6 (Male)	M	6	8	150	IP	Increased RAGE expression, p53/p21 upregulation
Wang et al., 2022[62]	Mouse/ Balb/c (Male)	M	11	8	150	IP	p16 protein expression increased relative to β-actin. Decrease in SOD
Cheng et al., 2021[95]	Rat/ Wistar (Male)	M	8	8	150	ROUTE NOT SPECIFIED	Significant increase in heart weight, ANP/BNP/β-MHC upregulated, Greater collagen deposition. IL-1β, IL-6, TNF-α Increase in concentration as well as pro fibrogenic protein expression such as Col-I, Col-III, α-SMA, TGF-β.

Bei et al., 2018[96]	Mouse/ C57BL/J6 (Male)	M	10 to 12	10	100	SC	increased $P16^{INK4a}$ and $P19^{ARF}$ expression. Decreased TRF1, TRF2, TERT expression. Upregulated miRs 1946a, 1946b, 3113, 21, 34c. EF%/FS% reduced. miR 21 Knockout prevented D-Gal induced aging phenotype and expression changes
Otsyula et al., 2003[97]	Rat/ Sprague-Dawley (Male)	M	175-200 (g) + 1 week acclimation	9	50% of Diet	PO	Significantly lower BW, NOT significant increase in AGEs. Activities of some antioxidant enzymes decreased compared to diabetic group. ONLY thiobarbituric acid reactive substances decreased compared to control.
Chen et al., 2019[98]	Mouse/ C57BL/J6 (Male)	M	8	8	0,150,300, and 600	SC	No BW Changes. Significant increase in expression of Fis1 in 300 mg group compared to WT saline control.
Hu et al., 2022[73]	Rat/ Wistar (Male)	M	8	TOTAL TREATMENT UNSPECIFIED	2000	IP	Disarrayed CM with more tissue gap. Increase in Fibrosis. Increase in p53 expression. Suppression of SOD.
Yi et al., 2020[99]	Mouse/ ICR (Mixed)	X	10	6	120	IP	Increase in MDA. Decrease in SOD. Organ indices decreased.

Liu et al., 2021[100]	Mouse/ C57BL/J6 (Male)	M	7	10	200	SC	BW decreased compared to control. Increase in AGEs. Increase in free fatty acids. Lipid peroxidation and Malonaldehyde levels increased in heart.
Li et al., 2016[68]	Rat/ Sprague-Dawley (Male)	M	200-220 (g) + 1 week acclimation	6	400	IP	Malondialdehyde and protein carbonyl levels increased. Glutathione levels significantly reduced. Antioxidative capacity (T-AOC, SOD, GSH-Px) significantly reduced.
Dehghani et al., 2019[101]	Rat/ Wistar (Male)	M	170-200 (g)	8	150	IP	Higher Mean Arterial Pressure. HW/BW rate significantly increased. Mn-SOD(SOD2) and Catalase mRNA levels reduced in heart. Malondialdehyde levels *dramatically* increased in heart.
Li et al., 2014[70]	Rat/ Sprague-Dawley (Male)	M	200-230 (g) + 1 week acclimation	10	150	SC	Significant increase in Saβ-Gal positive cells and AGEs, [Malondialdehyde levels up, Glutathione down, SOD/Catalase/Glutathione reductase activity down](SERUM and LIVER) H2O2 imcreased in liver. Implicates FOXO3a and Nrf2 Pathways in D-Gal induced aging.
Musick and Wells, 1974[102]	Rat/ Holtzman (Male)	M	350-400 (g)	N/A	N/A	Perfusion	Splits Metabolics/Kinetics through relevant Glactose processing enzymes between brain, liver, heart.

Wang et al., 2023[103]	Mouse/ C57BL/J6 (Male)	F	26	12	120	SC	Enlarged CM nucleus myocardial fibres loose and disordered. Increased collagen deposition. Increase in Saβ-GAL (+) cells% and expression of p53/p21/p16 relative to GAPDH.
Quan-Ma and Wells, 1965[104]	Rat/ Holtzman (Male)	M	Weanling	2	35% of Diet	PO	High cardiac concentration of galactitol
Yi et al., 2021[67]	Mouse/ ICR (Mixed)	X	6	6	120	IP	Decrease in expression of protein and mRNA of SOD1/SOD2/CAT in liver and spleen. Reduction in nNOS/eNOS expression. Increase in iNOS expression
Guo et al., 2020[105]	Mouse/ ICR (Mixed)	X	6	6	120	IP	D-Gal had lowered organ indices. Increased NO and MDA decreased SOD/GSH-Px/GSH/CAT in serum and liver.
El-Far et al., 2021[106]	Rat/ Wistar (Male)	M	120 ± 20 (g)	7	200	SC	Disarrayed necrotic myofibers. Lowered Bcl2 expression. High expression Casp-3. Upregulation of TP53, p21, and Bax.

El-Baz et al., 2019[74]	Rat/ Wistar (Male)	M	130–150 (g) + 1 week acclimation	8	200	IP	Increased HR/PR interval/QRS interval. Decreased ST height. Increased serum levels of Homocysteine cratinine kinase isozyme, and lactate dehydrogenase. Decrease in cardiac GLUT-4 marked elevation of IL-6 and iNOS. Increase in SOD and NF-κB. Downregulated RAR-α. Disarrayed cardiac structure.

2 METHODS

2.1 Animals

All experimental procedures were approved by the animal ethics and scientific committees at the Montreal Heart Institute in accordance with the Canadian Council on Animal Care guidelines (protocol numbers: 2022-47-07; 2023-47-08). In all experiments of this study, Wild-type (WT) Sprague Dawley (SD) were purchased from Charles-River (strain code: 001; Charles-River, St-Constant, QC) at 6 weeks of age to arrive for 7 weeks of age and acclimate before beginning treatment at 8 weeks of age. Rats were housed in pairs up to 500g of weight and separated when above. Rats were given access to a growth-focused diet (Envigo, Indianapolis, IN, 2018s) and water ad libitum and were housed in a temperature-controlled environment with a 12-hour light and 12-hour dark cycle.

2.2 Treatment

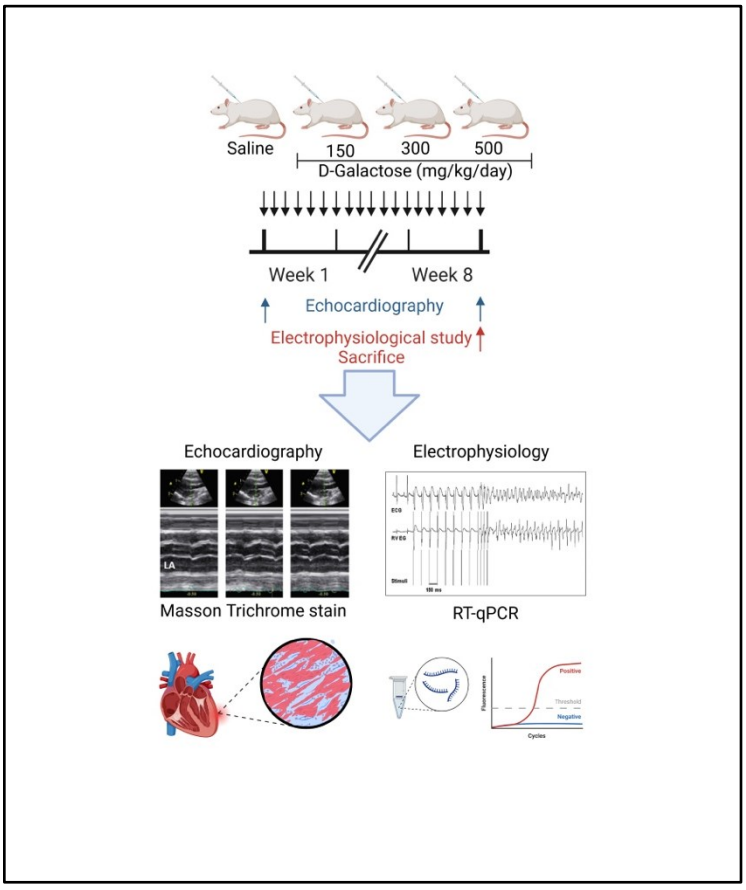

Figure 6. Graphical overview of experimental planning and procedure

Rat groups involved in the induced aging model testing experiments were injected daily subcutaneously in the rump with various dosages (150 [N = 36 total animals, n = 9 animals per sex per group], 300 [N = 18 total animals, n = 6 animals per sex per group], and 500 [N = 18 total animals, n = 6 animals per sex per group] mg/kg/day) of D-galactose (Sigma-Aldrich G0750-500G) dissolved in sterile 0.9% sodium chloride saline solution (Baxter, Mississauga, ON, JB1323) or an equivalent volume of sterile saline solution vehicle for 8 weeks. D-galactose solution was prepared according to the product solubility guidelines for groups treated with a 150 mg/kg/day dosage. For higher dosage groups solution was prepared to a

concentration of 250mg/mL and heated in an incubator (Bio-Rad, BR-150) at 50°C for 20 minutes to facilitate dissolution and subsequently allowed to cool down to room temperature. Prepared solutions were sterilised by being forced through a PALL® Acrodisc® 32mm syringe filter with 0.2µm Supor® membrane (PALL Life Sciences, 4652).

Rat groups involved in metabolism experiments [N=24 total animals, n=6 animals per sex per group] were arranged into groups using a balanced latin square to compensate for variability due to aging over the course of the repeated blood drawing experiment and accounts for both order- and carry-over effects (**Table 2**). Rats were injected subcutaneously in the rump with D-galactose dissolved in sterile 0.9% sodium chloride saline solution (250mg/mL, 500mg/kg/day) once per week and had 500µL of blood drawn from the tail vain using a butterfly catheter at one of the various studied time intervals (0.5-, 1-, 2-, 4-, 8-, and 12-hours post-injection).

Table 2. Example arrangement of rat group in a balanced latin square for blood drawing procedure

		WEEK					
		1	2	3	4	5	6
Hours Elapsed	0.5	A	B	F	D	E	C
	1	B	D	A	C	F	E
	2	D	C	B	E	A	F
	4	C	E	D	F	B	A
	8	E	F	C	A	D	B
	12	F	A	E	B	C	D

2.3 Transthoracic Echocardiography

Induction and maintenance of inhalation anaesthesia on rats undergoing the procedure was performed with 2% isoflurane and 100% oxygen (2L/min) and body temperature was maintained using an electric heating pad. The rats' thoraxes were then shaved, and depilatory cream was applied for four minutes followed by rinsing the cream off with warm water. During echocardiography recording body temperature was maintained using a Gaymar TP-700 water circulating heating pad (Paragon Medical, Coral Spring, FL). A surface lead II electrocardiogram was recorded with 30-g subdermal electrodes (Grass Technologies, West Warwick, RI) Echocardiogram capture utilised parasternal long-axis views to enable capture of both motion-mode and Doppler echocardiograms on a Vivid 7 Dimension System (GE, Healthcare Ultrasound, HO) Imaging and analysis were performed blinded to treatment group.

2.4 *In vivo* Electrophysiology

Inhalation anaesthesia was induced with 5% isoflurane and 100% oxygen (2L/min) and maintained at 2% isoflurane and 100% oxygen (2L/min) throughout the procedure. Body temperature was maintained using a water circulating heating pad (Paragon Medical, Coral Spring, FL). A skin incision was made, and the right pectoral muscle was carefully shifted to provide access to the inferior portion of the right external jugular vein. With the vein isolated, the superior portion was partially sutured, and a small perpendicular incision was made in the vein. A 1.9F octopolar electrophysiology catheter (Transonic Scisense, London, ON) was gently inserted into the vein, with catheter positioning assessed via coupled electrode recording to ensure the distal portion showed strong ventricular signals, the middle portion

His bundle activity, and the proximal portion strong atrial signals. All pacing was performed from the most proximal electrodes with threshold-current being measured through continuous pacing (1 msec pulse duration, cycle length (CL)=110 msec) while incrementally increasing voltage until the lowest voltage that maintained 1:1 atrial capture stimulation was observed. Three minutes rest was allotted after threshold-determination. Atrial effective refractory period (AERP) was measured by eight consecutive S1 stimuli (1 msec pulse duration, CL=100ms) followed by a single S2 stimulus and a two second pause. S2 stimulation varied from 100 msec to 10 msec, decreasing in two msec increments each time. The longest S2 stimulus that that failed to produce atrial activity was fixed as the AERP. Sinus node recovery time (SNRT) was recorded by stimulating the heart for thirty seconds of stimulation (1 msec pulse duration, CL=120ms) and measuring the duration between the final paced atrial and initial spontaneous sinoatrial node-induced P-wave. Correction for the SNRT was calculated by subtracting the paced CL from the average of the next 30 consecutive restored heartbeats. The Wenckebach point (WBP) was measured by eight consecutive stimulations (1 msec pulse duration) with a variable CL beginning just below the sinus rhythm CL and progressively decreasing the CL until paced atrial complexes failed to induce ventricular depolarization. The longest CL that failed to produce ventricular depolarization was fixed as the WBP. All parameters were analyzed using ecgAUTO v.3.5.5.25 (EMKA Technologies, Sterling, VA) and utilized a 60Hz electrical noise filter on the raw signal.

2.5 Euthanasia

Following the careful removal of the electrophysiology catheter, rats were deeply anaesthetised via inhalation of 5% isoflurane and 100% oxygen (2L/min). The rib cage was

then opened, and the heart grasped from the apex to avoid atrial damage. A 25G syringe was inserted to the right of the apex and one mL of blood was drawn out and left to coagulate for 10 minutes before being transferred into a 4°C refrigerator. After the blood was drawn, the aorta was sectioned and the heart was transferred to a Sylgard® coated dish filled with phosphate buffered saline solution (PBS) to wash the remaining blood. Hearts were randomly apportioned to either be sent for histological staining or RNA extraction. Hearts selected for histology were thoroughly washed and transferred to tissue cassettes and placed in a container filled with 10% formalin in PBS for 48 hours. Hearts selected for RNA extraction were pinned at the bottom of the dish and the atria were removed and stored separately. The heart was then flipped and pinned again to expose the posterior portion of the ventricles. The ventricles were then separated by cutting along the coronary sinus before separating the right and left ventricles and storing them separately. Tissue separated and selected for RNA extraction was immediately flash-frozen using liquid nitrogen.

2.6 mRNA isolation and quantitative polymerase chain reaction (qPCR)

LA tissue was homogenized with an isolation buffer for mRNA extraction following the manufacture's instructions (Macherey-Nagel, Düren, NRW). Complementary DNA (cDNA) was transcribed utilising the isolated mRNA in tandem with a high-capacity cDNA reverse transcription kit (Applied BioSystem, Waltham, MA) in a thermal cycler (Applied BioSystem, Waltham, MA, 2720). 20 ng duplicate samples of obtained cDNA were loaded into designated plates to perform qPCR with SYBRGreen® on select genes. Changes in fluorescence were quantified using a StepOnePlus Real-Time PCR machine (ABS, Waltham, MA).

2.7 Masson's trichrome stain

Tissues were removed from the 10% formalin and stored in 70% ethanol until embedding. Paraffin-embedded tissue was sectioned (10 μm) using a microtome on a frontal plane to expose tissue sections with whole heart slices with clearly identifiable atria and ventricles. Tissue sections were mounted on slides and Masson's trichrome staining was performed. To quantify fibrotic tissue area, images were captured with a microscope (Olympus, Tokyo, JPN, BX46) and collagen quantification was performed using ImageJ software (NIH, Washington D.C.).

2.8 D-galactose serum concentration enzyme linked immunosorbent assay (ELISA)

Collected blood was left at 4°C to congeal for an hour before being spun at 5000g for 10 minutes at 4°C in a centrifuge (Hettich Zentrifugen, Tuttlingen, BW, Universal 32R). Serum was then carefully separated from the precipitated red blood cells, and both were flash-frozen in liquid nitrogen and stored at -80°C until ready for use. When testing was performed serum samples were thawed and both vortexed and spun to ensure equal distribution. Samples were loaded onto a 96-well reader plate in triplicate and ELISA was run according to manufacturer's instructions (Thermo Fisher Scientific, EIAGALC).

2.9 Statistics

All quantitative data are displayed using a mean ± standard error of the mean (SEM). Statistical tests utilized include Student's t-test for analyses containing only two groups. Corresponding to the number of categorical variables, a one-way or two-way analysis of variance (ANOVA) was applied when groups compared numbered greater than two. Where

experimental design accounted for it, repeated measures ANOVA was used to reduce residual error. Where results benefitted from being compared to a relevant control, Dunnett's multiple comparisons test (MCT) was used to reduce risk of type I error. If all comparisons were made, Tukey's MCT was utilized for the same purpose. Normal distribution of the data was determined with the Kolmogorov-Smirnov distribution test. Use of statistical tests are specified in each corresponding figure or table description along with sample sizes where 'N' represents the total number of animals and 'n' the number of animals in each group.

3 RESULTS

3.1 Effect of D-galactose induced aging on AF vulnerability and electrophysiology in rats

Transjugular stimulation at twice threshold capture value induced AF in only one low dose treated male rat and one low dose control (**Figure 7A**). In medium and high dose groups only one male rat of the highest dose group displayed an induced AF event. Female rats showed no AF inducibility throughout all the groups (**Figure 7A-B**). Rarity of AF inducibility was reflected in the duration of events which ranged from the minimum threshold of event recording at 0.5 sec in the high dose male group to 1.5 sec in the low dose male control group (**Figure 7A-B**). Lack of AF inducibility in female groups did not allow for meaningful quantifiable AF duration data. Estimated refractory period (ERP) and corrected sinus node recovery time (cSNRT) showed no differences across all treatment groups in both males and females. ECG analysis yielded no significant changes to P-wave duration or amplitude, P-R or Q-T intervals, or QRS duration, across all treatment groups in both males and females (**Figure S1**).

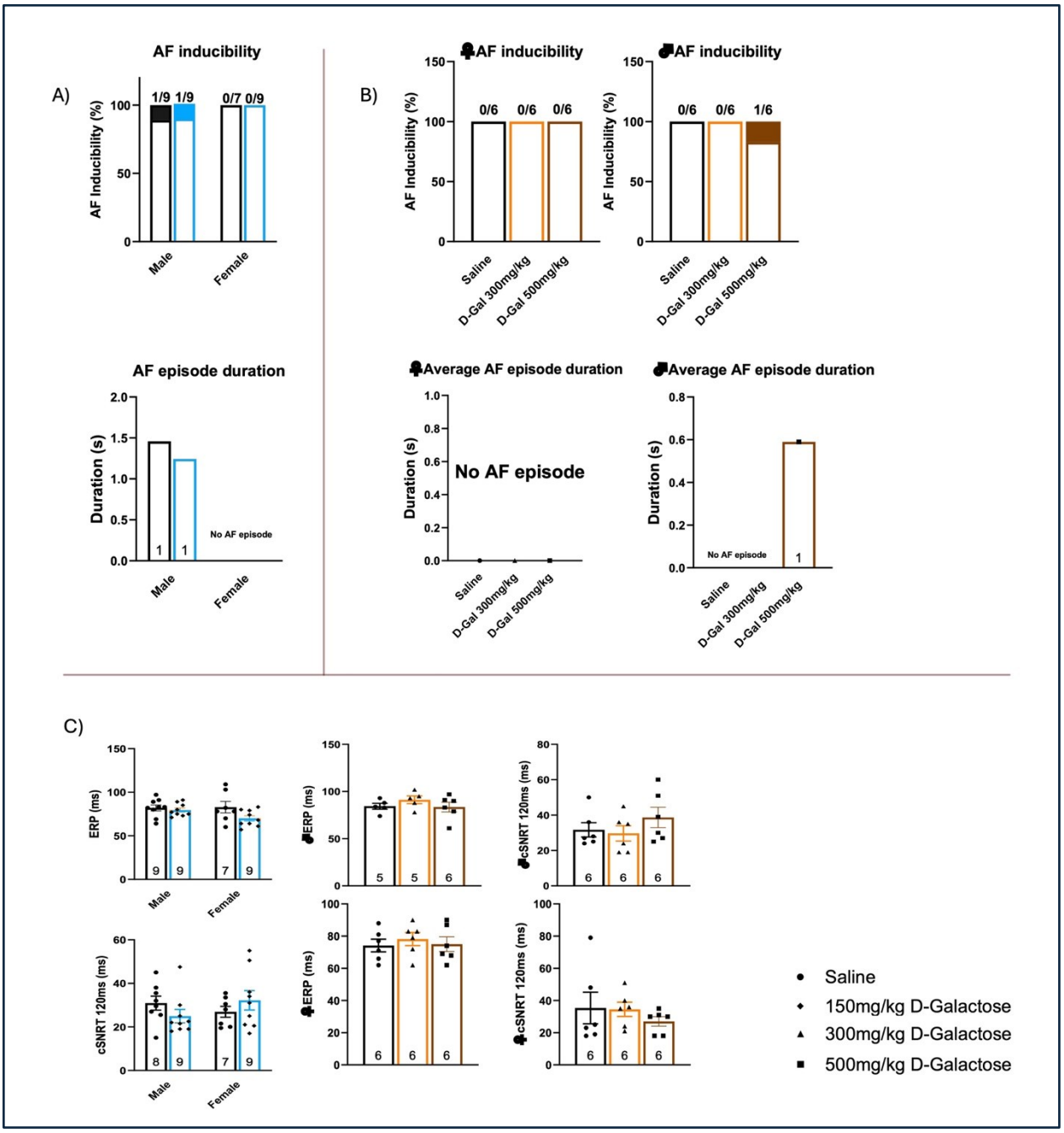

Figure 7. AF inducibility and Electrophysiology parameters in D-galactose and vehicle treated rats. A) *Percentage of rats showing atrial fibrillation inducibility and event duration from atrial burst pacing in 150mg/kg/day dosed groups (N=7-9)* ***B)*** *Percentage of rats showing atrial fibrillation inducibility and average fibrillation event duration per animal in 300mg/kg/day and 500mg/kg/day dosed groups* ***C)*** *Electrophysiological parameters recorded over all groups: ERP: estimated refractory period; cSNRT: corrected sinus node recovery time. (N=5-9)*

3.2 Cardiac functional and structural changes in D-galactose induced aging rats

In order to better elucidate the efficacy of the accelerated aging models, delta scores (baseline values subtracted from the endpoint values) were used to compare phenotype evolution over the course of treatment. Echocardiography analysis showed no significant difference in evolution over treatment of left atrial (LA) structural parameters [in both males and females] in the low dose experiments (**Figure 8**). Atrial fractional shortening (Atrial FS) delta scores were significantly increased in medium dose treated male rats compared to its control group, though there was no significant increase observed in the higher dose group, nor were there any significant changes over treatment in any of the atrial diameter measurements in any of the male groups (**Figure S2A**). No significant differences in evolution of atrial diameter or atrial FS were observed in the female groups (**Figure S2A**). Left Ventricular (LV) structural parameter delta scores were not significantly different between all groups (**Figure 8**, **Figure S2C**). Functional parameters such as Left Ventricular Ejection Fraction (LVEF) and Fractional Shortening (LVFS) did not evolve significantly over the treatment period in all groups (**Figure 8**). Variations of E-wave and A-wave speeds over treatment were not significant, nor were the differences of the delta scores in the E/A ratio or E-wave deceleration time (EDT) (**Figure S2B**). The LV dimensional parameter was not significantly altered over the course of treatment (**Figure 8**, **Figure S2C**).

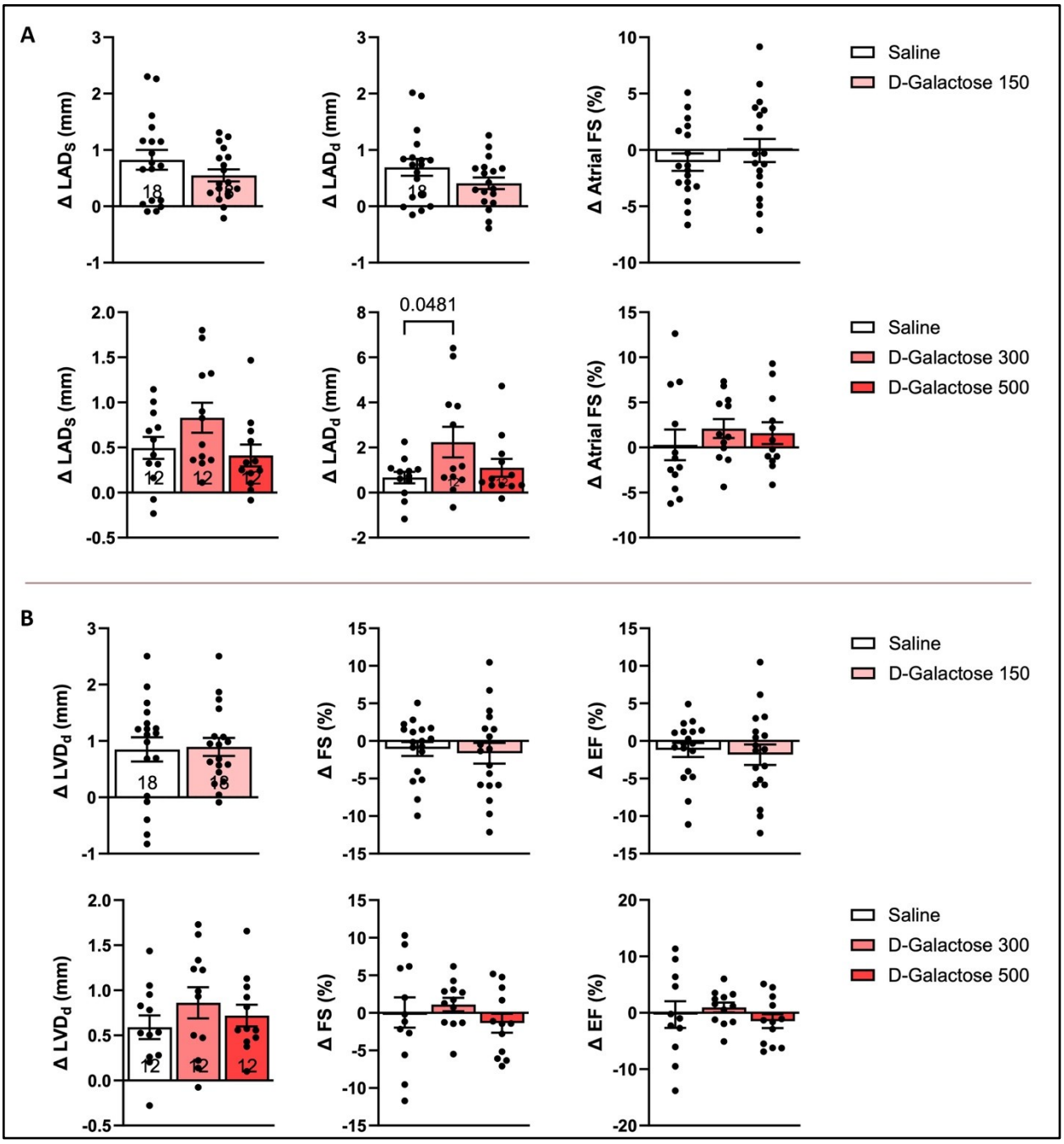

Figure 8. Echocardiographic data of D-galactose treated, and vehicle treated rats. A) *Changes in left atrial dimensional parameters over all groups: LADs - left atrial dimension at end of systole; LADd - left atrial dimension at end of diastole; Atrial FS: overall atrial fractional shortening.* ***B)*** *left ventricular systolic functional and structural parameter changes over all groups: LVDd: left ventricle dimension at end of diastole. FS%: Left ventricular fractional shortening. EF%: Left ventricular ejection fraction. Statistical analysis: Low dose group: unpaired t-test, significance level P<0.05. Medium and High dose groups: one-way ANOVA ; Dunnett's multiple comparisons test, significance level P<0.05.*

3.3 Fibrosis and related marker quantification in D-galactose induced aging rats

Masson's trichrome staining revealed no significant differences in the percent collagen of observed tissue area in the LA or in any of the other heart quadrants observed (**Figure 9**, **Figure S4**). Fibrosis related genes *Col1a1*, *Col3a1*, and *Mmp9* mRNA were quantified, but there were no significant differences between low dose groups (**Figure 9**). Analysis of *Col1a1* expression in medium and high dose groups did not reveal any statistically significant differences either (**Figure S5**).

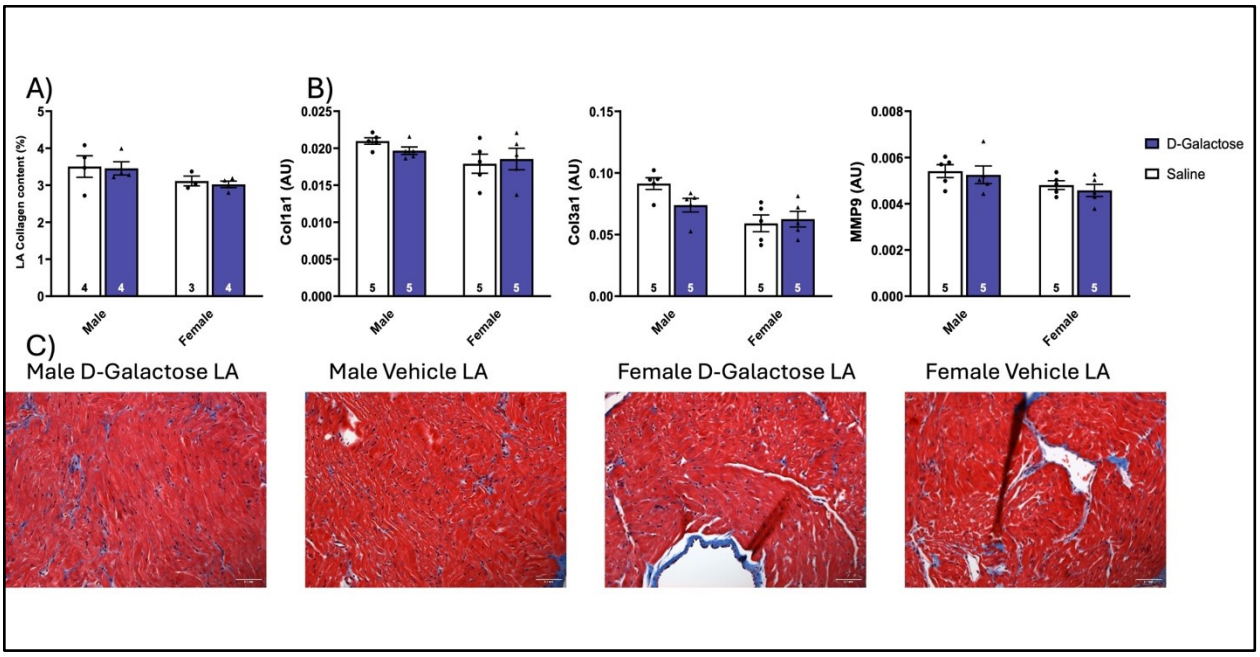

Figure 9. Fibrosis quantification and fibrosis-associated gene mRNA changes in low dose regimen rats. A) *Analysis of left atrium stained with Masson's Trichrome stain. Graph displays mean ± SEM fibrosis as a percentage of cross-sectional area of tissue. Each point represents an individual animal (N=3-4) (statistical analysis: two-way ANOVA ; Bonferroni multiple comparisons test, significance level p<0.05)* ***B)*** *Messenger RNA expression, measured by qPCR and expressed in arbitrary units (A.U.) for fibrosis markers Col 1a1, Col 3a1, Mmp9. Normalized to the geometric mean of the threshold cycle value of three housekeeping genes: B2m, Gapdh, and Hprt. (N=5) (statistical analysis: two-way ANOVA ; Tukey's multiple comparisons test, significance level P<0.05)* ***C)*** *Representative images of left atrial tissue.*

3.4 Expression of senescence associated markers in D-galactose induced aging rats

qPCR quantified expression levels of mRNA for senescence markers *p16*, *p21*, *p53*, and *Glb1* showed no difference between low dose groups (**Figure 10**). Select genes associated with cell-survival and apoptosis, inflammation, and extracellular matrix remodeling were also quantified, though no significant differences emerged between the low dose groups (**Figure S3**). In medium and high dose group experiments, female rats treated with medium dose D-galactose displayed a significant increase in *p21* mRNA expression compared to its control, but there was no significant difference observed in the high dose female group or in any of the other senescence genes analyzed (**Figure 10**). No significant differences in senescence associated genes were observed in the male groups treated with the medium- or high-dose regimen (**Figure 10**). Inflammation associated genes analyzed in the medium- and high-dose groups were not significantly different from their associated controls over all groups (**Figure S5**).

-

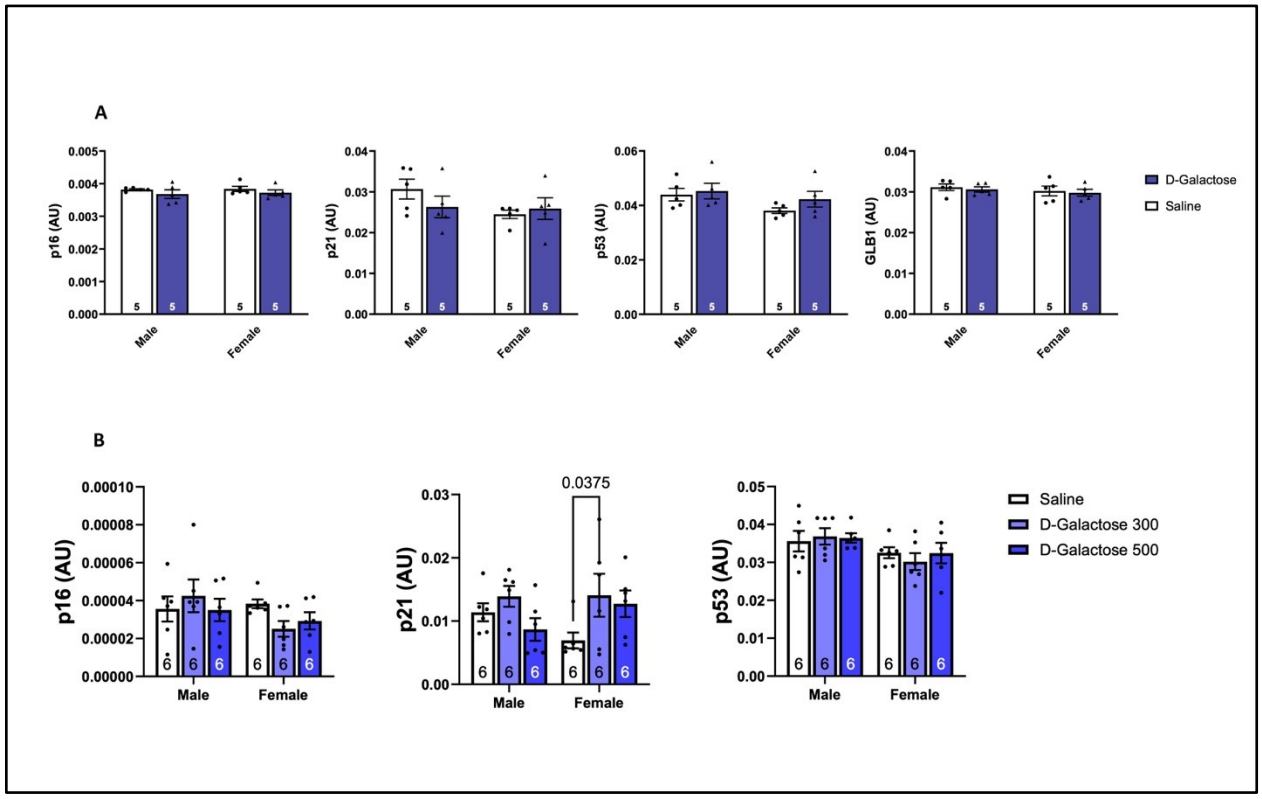

Figure 10. mRNA expression of senescence markers in treated versus untreated rats. A) *Senescence markers, p16, p21, p53, Glb1 in LA of low dose rats. Normalized to the geometric mean of the threshold cycle value of three housekeeping genes: B2m, Gapdh, and Hprt. (N=5) (statistical analysis: two-way ANOVA ; Tukey's multiple comparison test, significance level P<0.05)* ***B)*** *Senescence markers, p16, p21, p53 in LA of medium and high dose rats. Normalized to the geometric mean of the threshold cycle value of three housekeeping genes: B2m, Gapdh, and Hprt. (N=5) (statistical analysis: two-way ANOVA ; Dunnett's multiple comparison test, significance level P<0.05)*

3.5 Changes in serum concentration of D-galactose upon administration of D-galactose to rats

ELISA quantification of serum concentration of D-galactose was employed to confirm proper administration of D-galactose over the course of treatment and assess the model viability for further experimentation. Significant spikes in serum D-galactose concentration were observed shortly after injection in female rats at 0.5-hours (p=0.022) and 1-hour post-injection (p=0.0119) and slightly delayed at 1-hour post-injection (p=0.0135) in male rats. By

2-hours after D-galactose administration, neither male nor female groups had serum concentrations that differed significantly from their control counterparts. All other timepoints measured through to 24-hours post-injection yielded no significant differences between all groups (**Figure 11**).

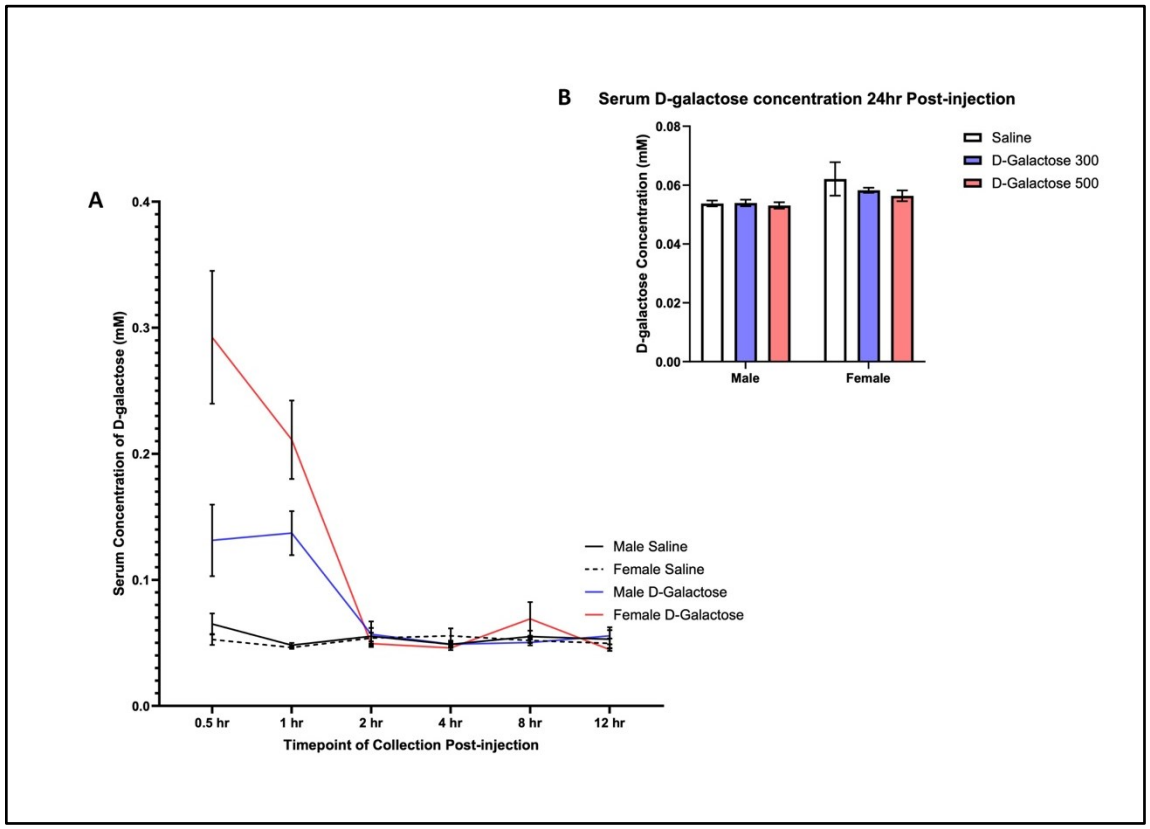

Figure 11. Serum concentration of D-galactose metabolism over time in rats injected with D-galactose or vehicle. A) *Time course measured change in serum concentration levels post-injection of high dose regimen (500mg/kg/day). Mean ± SEM (N=6). Statistical analysis: two-way repeated measures ANOVA ; Tukey's multiple comparisons test, significance level p<0.05.* ***B)*** *Concentration of D-galactose in serum 24hr after the end of 8-week high and medium dose treatment regimen. Mean ± SEM (N=6) Statistical analysis: two-way ANOVA ; Dunnett's multiple comparison test, significance level p<0.05.*

4 DISCUSSION

4.1 Novel Findings

Our study focused on extending and standardizing the reported models of D-galactose induced cardiac aging phenotypes to induce the development of AF. However, our findings stand in contrast to much of the literature and display that no induction of any aging-like phenotype was observed as the outcome of the implementation of the D-galactose aging model. We confirmed our methodology and accuracy of our results using experimental kinetics and show that the model framework as described remains unable to produce reported outcomes. To our knowledge this is the first study that has tracked the consequences of D-galactose administration in the heart over long term administration and provided a robust set of measurements to evaluate the model's ineffectiveness.

4.2 Understanding experimental outcomes

4.2.1 Atrial fibrillation

The foremost outcome to be acknowledged, is that we were unable to standardize D-galactose administration in a manner that allowed for the reliable induction of AF in rats even at the high dose regimen of 500mg D-galactose per kilogram of body weight per day. This runs counter to a recent study conducted by Zhang et al. investigating whether gut microbes can be targeted to prevent age-related AF. The authors utilized D-galactose administration to induce senescence and structural remodelling and reported AF inducibility with a dose of 150mg of D-galactose per kilo per day.[63] To our knowledge, this is the only study that reported AF inducibility as an outcome of D-galactose administration to date.

4.2.2 Cardiac changes and an evaluation of aging-related changes

Our experimentation yielded no significant differences in structural and functional heart parameters in treated rats at all dosages and over both sexes. This ran contrary to our initial expectations for this model, hoping that - in accordance with published literature - a cardiac aging phenotype potentially accompanied by AF inducibility would be observed. Aging studies performed by Mehdizadeh et al. (unpublished data), with whom we shared both animal procurement as well as housing and handling protocols, recorded the phenotypic and functional differences between 20-month-old and 3-month-old Sprague Dawley rats. They observed significant increases in both atrial and ventricular diameters with age, as well as decreases in cardiac function such as reduced ejection fraction. Furthermore, characteristic changes in inflammation observed with aging were present in aged animals in the Mehdizadeh et al. (unpublished data) experiments, while absent from our own induced aging model. In addition, gene expression results cataloguing senescence were visibly more consistent in naturally aged rats than what was observed through induced senescence modelling with D-galactose in the current study.[107] While both studies cannot be statistically combined and compared, the lack of similar trends and directions to those observed between young and naturally aged rats raises questions as to the effectiveness of the model's ability to replicate physiological changes observed in natural aging.

4.3 Comparison with the reported literature

Though only one paper reported AF inducibility as an outcome of D-galactose administration, many have reported some changes to cardiac structure and functionality. (**Table 1**) Chang et al., Bo-Htay et al., and Hong et al. all administered D-galactose at a

dosage equivalent to our low dose of 150mg/kg/day and reported significant reductions in EF% and FS%.[72,77,78] Zhang et al. and Bei et al. reported reduced EF% and FS% with dosages as low as 125 and 100 mg/kg/day respectively.[91,96] Meanwhile, all three of our tested doses, equivalent to or above the aforementioned dosages, failed to induce a change in EF% or FS%. Some studies with more molecular focuses analyzed the effect of D-galactose administration on expression of senescence markers and reported mixed results in elevations of *p53*, *p26*, and *p21*. Bei et al. and Ji et al. reported increased *p16* expression, but no increase in the *p53/p21* pathway of senescence.[66,96] Conversely, Wang et al., Zhang et al., Maharajan and Cho, Maharajan et al., and Hu et al. all reported upregulation of *p53* and *p21* senescence marker expression, without observing changes to *p16*.[61,63,64,69,73] Only Wang et al. reported increased protein levels (relative to GAPDH housekeeping) of all three markers of senescence, however, mRNA expression was not investigated.[103] While we did not perform protein level expression experiments, our mRNA results displayed no difference of expression of senescent markers scaled to dosage across both sexes with the exception of the medium dose treated female group, and solely for the expression of *p21*. Deviations from published results also occurred in the mRNA expression levels of inflammation and fibrosis associated genes. We observed no upregulation of *Col1a1* or *Il-6* across all treatment groups and no significant changes to the expression of inflammation related genes *Il-1β*, *Tnfα*, and *Nlrp3* or fibrosis related genes *Col3a1*, *Mmp9*, and *Tgfβ2* compared to their control counterparts. Within the reported literature, however, Maharajan and Cho, Cheng et al., and Zhang et al. all report increased expression of *Il-6* and *Il-1β*. Cheng et al., and Zhang et al.

further recorded elevated *Tnfα* expression as well as fibrosis associated genes *Col1a1*, *Col3a1*, and *Tgfβ*.[63,64,95]

4.4 Questions of model effectiveness

Recently a growing number of research groups in a variety of fields have reported failure to induce aging or senescence using the D-galactose administration model. A study focusing on age-related hearing loss performed by Park et al. on mice, administering an equivalent dosage of our high dose group of 500 mg/kg/day, noted that D-galactose alone was not potent enough to induce age-related changes without combining it with other models of oxidative damage induction.[92] Similarly, Cardoso et al. attempted to accelerate aging using an equivalent to our medium dose group of 300 mg/kg/day to track neurodegeneration in rats, but reported failure to induce aging.[108] Furthermore, zooming out and appreciating the majority of the reported literature as a whole (**Table 1**) yields the question as to why there is no emergent pattern or consistent and standardized validation and application of the model. In fact, there are wide ranges on important metrics. When evaluating the effect of accelerated aging, it becomes important to have a normalized starting age by which to cross compare. In the application of these studies however, treatment begins as early as 4 weeks of age and as late as 22 weeks of age in rats alone.[76,89] Given that rats develop rapidly, reaching sexual maturity around six weeks of age, and that two weeks of a rats life corresponds to roughly a human year, such a vast range of difference in treatment onset ages can impact whether changes observed are truly a function of accelerated aging.[109] Overall, treatment duration ranged from four weeks to 88 weeks and dosages of as low as 50mg/kg/day all the way up to 2000mg/kg/day were injected, using various administration

routes.[66,71,73,87] Both of these metrics when non-standardized dilute the value of the recorded results, as readers cannot possibly evaluate the degree of damage due to the compound or treatment regimen versus the effects of time elapsed or osmotic pressure in and of itself. Another emergent issue from evaluating the literature as a whole is, the noticeable amount of omission of information. Studies that purport to find effective use of the model fail to disclose crucial information such as age of treatment onset, dosage, or duration. It's with these vagaries in mind that help frame the understanding of our metabolic experiments.

4.5 Viewing the D-galactose administration model through metabolism

The reported framework for D-galactose administration is on a per day basis. With this in mind, we sought to capture a sense of metabolism over a 24-hour period. Observing that serum levels returned to basal levels within two hours of administration in both male and female groups, as well as observing no residual serum D-galactose in treated rats at the end of 8 weeks, led us to suspect that in light of the absence of structural and functional changes toxic buildup resulting from excess D-galactose was not occurring. Thus, even if cellular damage was occurring in cardiac tissue over the two hours of exposure, enough time had elapsed to allow for repair before the next injection was to be administered on the 24-hour cycle. If this is true, then regardless of the duration of treatment there is a high likelihood that at our dosages – which have been selected to cover the majority of dosages reported in the literature – no effect would be observed.

Furthermore, it has been demonstrated in a variety of rat studies on other organs, that the assumed severe oxidative stress caused by D-galactose induced ROS accumulation may not

be the sole outcome of D-galactose exposure. In fact, several studies have shown that D-galactose administration produces a concomitant neuroprotective effect and even reverses cognitive impairment in rodent Alzheimer's disease models. In effect, even with the initial increase in ROS induced by D-galactose, subsequently activated cellular defense mechanisms against oxidative stress seem to produce a net positive outcome.[110–113] Additionally, a different study by Homolak et al. showed similar results in a time-course study when investigating acute effects of orally administered D-galactose in the intestine of rats.[114] Indeed, as touched upon above and by other authors, the lack of standardization together with a dearth of investigation as to the sum total of effects on the cellular level within various organs may be at the root of the variability within the outcomes observed from the model implementation (**Table 1**).[114,115] The assumed association of D-galactose administration and oxidative stress outcomes informs much of experimental design in studies that employ D-galactose administration, however, the underlying mechanisms and even the association itself is seldom evaluated. Notably, the induction of oxidative stress through enzymatic processing via galactose oxidase touted in metabolic mechanism overviews fails to note that this particular enzyme is of fungal origin and thus not expressed in mammals.[116]

4.6 Limitations

The limitations of our experimentation are important to consider when evaluating outcomes compared to that of the existent literature. Importantly, we did not perform any naturally aged rat experiments, which would have lent greater strength to our comparisons. When compared to other experiments performed throughout the literature, we were unable to

assess certain findings and outcomes, as we did not perform Western Blots to evaluate protein expression separately from mRNA level changes, nor did we do any direct ROS or AGE detection experiments. Furthermore, the scope of our study was limited to assessing changes in the heart, and thus our findings cannot evaluate the effects of the model in other organ systems. While we were able to show that D-galactose is metabolized rapidly by showing that blood concentrations decreased to undetectable over a matter of hours, we did not verify D-galactose or its metabolites' direct concentrations in the heart (e.g. via HPLC-MS) which would give a more holistic understanding of their direct effect on the heart and to what extent tissue uptake versus excretion plays a role in the model's effectiveness. RNA sequencing could provide a better overview of changes due to D-galactose administration rather than targeted qPCR.

4.7 Conclusions and future directions

The present study shows that contrary to most reports, 24-hour cycled administration of D-galactose is not effective in inducing an aging-like cardiac phenotype, cellular senescence, or any cardiac arrhythmia in rats when compared to their control counterparts. It also displays the various barriers to a viable standardized model by being of the first to analyze absorption of D-galactose over the short and long term and casts light on the need for rigorous review and replicability of the reported literature in line with the growing number of researchers reporting model ineffectiveness. Further work should be done to identify the interval of administration, if any, at which the model begins to properly display desired effects. It may be necessary to administer the compound much more frequently to reproduce senescent changes. It's important to make clear that the use as an ease-of-

access accelerated aging model may be compromised with the need to re-administer D-galactose at short intervals and the role of D-galactose administration in aging research may be negated by confirming these findings. While a D-galactose administration model, once standardized and fully studied, could potentially be used to induce specific symptomatic changes in different organs and tissues, precaution should be used when stating that it can reliably reproduce the very complex – and as of today not fully understood – process of aging. Thus, for each age-related phenotype studied, validation that D-galactose administration can efficiently reproduce relevant hallmarks when compared to naturally aged counterparts should be conducted before this model is employed.

5 REFERENCES

1. Cardarilli, G. C., Di Nunzio, L., Fazzolari, R., Re, M. & Silvestri, F. Improvement of the Cardiac Oscillator Based Model for the Simulation of Bundle Branch Blocks. *Applied Sciences* **9**, 3653 (2019).

2. Joyner, M. J. & Casey, D. P. Regulation of Increased Blood Flow (Hyperemia) to Muscles During Exercise: A Hierarchy of Competing Physiological Needs. *Physiological Reviews* **95**, 549–601 (2015).

3. Park, D. S. *et al.* Ionic Mechanisms of Impulse Propagation Failure in the FHF2-Deficient Heart. *Circulation Research* **127**, 1536–1548 (2020).

4. Nattel, S., Maguy, A., Le Bouter, S. & Yeh, Y.-H. Arrhythmogenic Ion-Channel Remodeling in the Heart: Heart Failure, Myocardial Infarction, and Atrial Fibrillation. *Physiological Reviews* **87**, 425–456 (2007).

5. Padala, S. K., Cabrera, J. & Ellenbogen, K. A. Anatomy of the cardiac conduction system. *Pacing Clinical Electrophis* **44**, 15–25 (2021).

6. Benjamin, E. J. *et al.* Impact of Atrial Fibrillation on the Risk of Death: The Framingham Heart Study. *Circulation* **98**, 946–952 (1998).

7. Nattel, S. New ideas about atrial fibrillation 50 years on. *Nature* **415**, 219–226 (2002).

8. Elliott, A. D., Middeldorp, M. E., Van Gelder, I. C., Albert, C. M. & Sanders, P. Epidemiology and modifiable risk factors for atrial fibrillation. *Nat Rev Cardiol* **20**, 404–417 (2023).

9. Gao, P., Gao, X., Xie, B., Tse, G. & Liu, T. Aging and atrial fibrillation: A vicious circle. *International Journal of Cardiology* **395**, 131445 (2024).

10. Matsuoka, S. *et al.* Age Modified Relationship Between Modifiable Risk Factors and the Risk of Atrial Fibrillation. *Circ: Arrhythmia and Electrophysiology* **15**, e010409 (2022).

11. Andrade, J. G. *et al.* The 2020 Canadian Cardiovascular Society/Canadian Heart Rhythm Society Comprehensive Guidelines for the Management of Atrial Fibrillation. *Canadian Journal of Cardiology* **36**, 1847–1948 (2020).

12. O'Reilly, D. J. *et al.* The Burden of Atrial Fibrillation on the Hospital Sector in Canada. *Canadian Journal of Cardiology* **29**, 229–235 (2013).

13. January, C. T. *et al.* 2014 AHA/ACC/HRS Guideline for the Management of Patients With Atrial Fibrillation: A Report of the American College of Cardiology/American Heart Association Task Force on Practice Guidelines and the Heart Rhythm Society. *Circulation* **130**, (2014).

14. Jansen, H. J., Bohne, L. J., Gillis, A. M. & Rose, R. A. Atrial remodeling and atrial fibrillation in acquired forms of cardiovascular disease. *Heart Rhythm O2* **1**, 147–159 (2020).

15. Iwasaki, Y., Nishida, K., Kato, T. & Nattel, S. Atrial Fibrillation Pathophysiology: Implications for Management. *Circulation* **124**, 2264–2274 (2011).

16. Al Ghamdi, B. & Hassan, W. Atrial Remodeling And Atrial Fibrillation: Mechanistic Interactions And Clinical Implications. *J Atr Fibrillation* **2**, 125 (2009).

17. Daoud, E. G. *et al.* Effect of Atrial Fibrillation on Atrial Refractoriness in Humans. *Circulation* **94**, 1600–1606 (1996).

18. Chen, Z.-S., Tan, H.-W., Song, H.-M., Xu, W.-J. & Liu, X.-B. Impact of corrected sinus node recovery time in predicting recurrence in patients with paroxysmal atrial fibrillation. *J Int Med Res* **49**, 03000605211010103 (2021).

19. Whitbeck, M. G. *et al.* QRS duration predicts death and hospitalization among patients with atrial fibrillation irrespective of heart failure: evidence from the AFFIRM study. *Europace* **16**, 803–811 (2014).

20. Holmqvist, F. *et al.* Heart rate is associated with progression of atrial fibrillation, independent of rhythm. *Heart* **101**, 894–899 (2015).

21. Morseth, B. *et al.* Physical activity, resting heart rate, and atrial fibrillation: the Tromsø Study. *Eur Heart J* **37**, 2307–2313 (2016).

22. Kranert, M. *et al.* Recurrence of Atrial Fibrillation in Dependence of Left Atrial Volume Index. *In Vivo* **34**, 889–896 (2020).

23. Pan, N.-H., Tsao, H.-M., Chang, N.-C., Chen, Y.-J. & Chen, S.-A. Aging Dilates Atrium and Pulmonary Veins. *Chest* **133**, 190–196 (2008).

24. Platonov, P. G. Atrial fibrosis: an obligatory component of arrhythmia mechanisms in atrial fibrillation? *J Geriatr Cardiol* **14**, 233–237 (2017).

25. Yue, L., Xie, J. & Nattel, S. Molecular determinants of cardiac fibroblast electrical function and therapeutic implications for atrial fibrillation. *Cardiovascular Research* **89**, 744–753 (2011).

26. Gazoti Debessa, C. R., Mesiano Maifrino, L. B. & Rodrigues De Souza, R. Age related changes of the collagen network of the human heart. *Mechanisms of Ageing and Development* **122**, 1049–1058 (2001).

27. Xiao, S. *et al.* Cellular senescence: a double-edged sword in cancer therapy. *Front. Oncol.* **13**, 1189015 (2023).

28. Muñoz-Espín, D. *et al.* Programmed Cell Senescence during Mammalian Embryonic Development. *Cell* **155**, 1104–1118 (2013).

29. Kirkland, J. L. & Tchkonia, T. Senolytic drugs: from discovery to translation. *J Intern Med* **288**, 518–536 (2020).

30. McHugh, D. & Gil, J. Senescence and aging: Causes, consequences, and therapeutic avenues. *Journal of Cell Biology* **217**, 65–77 (2018).

31. Weintraub, S. J., Prater, C. A. & Dean, D. C. Retinoblastoma protein switches the E2F site from positive to negative element. *Nature* **358**, 259–261 (1992).

32. Zhao, S., Chen, Z., Han, S. & Wu, H. Effects of the p16/cyclin D1/CDK4/Rb/E2F1 pathway on aberrant lung fibroblast proliferation in neonatal rats exposed to hyperoxia. *Exp Ther Med* **22**, 1057 (2021).

33. Takasugi, M., Yoshida, Y. & Ohtani, N. Cellular senescence and the tumour microenvironment. *Molecular Oncology* **16**, 3333–3351 (2022).

34. Childs, B. G., Durik, M., Baker, D. J. & Van Deursen, J. M. Cellular senescence in aging and age-related disease: from mechanisms to therapy. *Nat Med* **21**, 1424–1435 (2015).

35. Cui, S. *et al.* Postinfarction Hearts Are Protected by Premature Senescent Cardiomyocytes Via GATA4-Dependent CCN1 Secretion. *JAHA* **7**, e009111 (2018).

36. Anderson, R. *et al.* Length-independent telomere damage drives post-mitotic cardiomyocyte senescence. *The EMBO Journal* **38**, e100492 (2019).

37. Shimizu, I. & Minamino, T. Cellular senescence in cardiac diseases. *J Cardiol* **74**, 313–319 (2019).

38. Martini, H. *et al.* Aging induces cardiac mesenchymal stromal cell senescence and promotes endothelial cell fate of the CD90 + subset. *Aging Cell* **18**, e13015 (2019).

39. Ferrucci, L. & Fabbri, E. Inflammageing: chronic inflammation in ageing, cardiovascular disease, and frailty. *Nat Rev Cardiol* **15**, 505–522 (2018).

40. Franceschi, C., Garagnani, P., Parini, P., Giuliani, C. & Santoro, A. Inflammaging: a new immune–metabolic viewpoint for age-related diseases. *Nat Rev Endocrinol* **14**, 576–590 (2018).

41. Barcena, M. L., Aslam, M., Pozdniakova, S., Norman, K. & Ladilov, Y. Cardiovascular Inflammaging: Mechanisms and Translational Aspects. *Cells* **11**, 1010 (2022).

42. Miwa, S., Kashyap, S., Chini, E. & Von Zglinicki, T. Mitochondrial dysfunction in cell senescence and aging. *Journal of Clinical Investigation* **132**, e158447 (2022).

43. Singh, V., Satheesh, S. V., Raghavendra, M. L. & Sadhale, P. P. The key enzyme in galactose metabolism, UDP-galactose-4-epimerase, affects cell-wall integrity and morphology in Candida albicans even in the absence of galactose. *Fungal Genetics and Biology* **44**, 563–574 (2007).

44. Caputto, R. & Leloir, L. R. The enzymatic transformation of galactose into glucose derivatives. *J Biol Chem* **179**, 497 (1949).

45. Robinson, B. H., Petrova-Benedict, R., Buncic, J. R. & Wallace, D. C. Nonviability of cells with oxidative defects in galactose medium: A screening test for affected patient fibroblasts. *Biochemical Medicine and Metabolic Biology* **48**, 122–126 (1992).

46. Murphy, M. P. How mitochondria produce reactive oxygen species. *Biochemical Journal* **417**, 1–13 (2009).

47. TeSlaa, T., Ralser, M., Fan, J. & Rabinowitz, J. D. The pentose phosphate pathway in health and disease. *Nat Metab* **5**, 1275–1289 (2023).

48. Coelho, A. I., Berry, G. T. & Rubio-Gozalbo, M. E. Galactose metabolism and health: *Current Opinion in Clinical Nutrition and Metabolic Care* **18**, 422–427 (2015).

49. Bo-Htay, C., Palee, S., Apaijai, N., Chattipakorn, S. C. & Chattipakorn, N. Effects of d-galactose-induced ageing on the heart and its potential interventions. *J Cell Mol Med* **22**, 1392–1410 (2018).

50. Azman, K. F. & Zakaria, R. d-Galactose-induced accelerated aging model: an overview. *Biogerontology* **20**, 763–782 (2019).

51. Wang, S. *et al.* D-galactose-induced cardiac ageing: A review of model establishment and potential interventions. *J Cellular Molecular Medi* **26**, 5335–5359 (2022).

52. Cavalera, M., Wang, J. & Frangogiannis, N. G. Obesity, metabolic dysfunction, and cardiac fibrosis: pathophysiological pathways, molecular mechanisms, and therapeutic opportunities. *Translational Research* **164**, 323–335 (2014).

53. Wong, C. W., Wong, T. Y., Cheng, C.-Y. & Sabanayagam, C. Kidney and eye diseases: common risk factors, etiological mechanisms, and pathways. *Kidney International* **85**, 1290–1302 (2014).

54. Taura, T. & Reddy, V. N. Effect of Sodium Iodate Injection on the Development of Galactose Cataract in the Rat. *Ophthalmic Res* **20**, 286–292 (1988).

55. Gona, O. & Gorelli, L. Mitosis in the lens epithelium of the galactose-fed rat after prolactin treatment. *Current Eye Research* **4**, 59–63 (1985).

56. Unakar, N., Tsui, J. & Johnson, M. Aldose reductase inhibitors and prevention of galactose cataracts in rats. *Invest Ophthalmol Vis Sci* **30**, 1623–1632 (1989).

57. Song, X., Bao, M., Li, D. & Li, Y. M. Advanced glycation in d-galactose induced mouse aging model. *Mechanisms of Ageing and Development* **108**, 239–251 (1999).

58. Cui, X. *et al.* D-Galactose-caused life shortening in Drosophila melanogaster and Musca domestica is associated with oxidative stress. *Biogerontology* **5**, 317–326 (2004).

59. Kumar, D. & Rizvi, S. I. Plasma paraoxonase 1 arylesterase activity in d-galactose-induced aged rat model: correlation with LDL oxidation and redox status. *Aging Clin Exp Res* **26**, 261–267 (2014).

60. Cui, X., Li, W. & Zhang, B. [Studies on cell senescence induced by D-galactose in cultured neurons and fibroblasts]. *Zhongguo Ying Yong Sheng Li Xue Za Zhi* **13**, 131–133 (1997).

61. Wang, S. *et al.* Activation of M3 Muscarinic Acetylcholine Receptors Delayed Cardiac Aging by Inhibiting the Caspase-1/IL-1β Signaling Pathway. *Cell Physiol Biochem* **49**, 1249–1257 (2018).

62. Wang, B. *et al.* Long-Term Social Isolation-Induced Autophagy Inhibition and Cell Senescence Aggravate Cognitive Impairment in D(+)Galactose-Treated Male Mice. *Front. Aging Neurosci.* **14**, 777700 (2022).

63. Zhang, Y. *et al.* Bacteroides fragilis prevents aging-related atrial fibrillation in rats via regulatory T cells-mediated regulation of inflammation. *Pharmacological Research* **177**, 106141 (2022).

64. Maharajan, N. & Cho, G.-W. Camphorquinone Promotes the Antisenescence Effect via Activating AMPK/SIRT1 in Stem Cells and D-Galactose-Induced Aging Mice. *Antioxidants* **10**, 1916 (2021).

65. Chang, Y. *et al*. *Alpinia oxyphylla* Miq extract ameliorates cardiac fibrosis associated with D-galactose induced aging in rats. *Environmental Toxicology* **34**, 172–178 (2019).

66. Ji, M. *et al*. Comparison of naturally aging and D-galactose induced aging model in beagle dogs. *Exp Ther Med* (2017) doi:10.3892/etm.2017.5327.

67. Yi, R. *et al*. The Impact of Antarctic Ice Microalgae Polysaccharides on D-Galactose-Induced Oxidative Damage in Mice. *Front. Nutr.* **8**, 651088 (2021).

68. Li, X. *et al*. Protective Effects of Selenium, Vitamin E, and Purple Carrot Anthocyanins on d-Galactose-Induced Oxidative Damage in Blood, Liver, Heart and Kidney Rats. *Biol Trace Elem Res* **173**, 433–442 (2016).

69. Maharajan, N. *et al*. Licochalcone D Ameliorates Oxidative Stress-Induced Senescence via AMPK Activation. *IJMS* **22**, 7324 (2021).

70. Li, Y.-N. *et al*. Saponins from *Aralia taibaiensis* Attenuate D-Galactose-Induced Aging in Rats by Activating FOXO3a and Nrf2 Pathways. *Oxidative Medicine and Cellular Longevity* **2014**, 1–13 (2014).

71. Lin, H. *et al*. D-galactose-induced toxicity associated senescence mitigated by alpinate oxyphyllae fructus fortified adipose-derived mesenchymal stem cells. *Environmental Toxicology* **36**, 86–94 (2021).

72. Hong, Y.-X. *et al*. Cardiac senescence is alleviated by the natural flavone acacetin via enhancing mitophagy. *Aging* **13**, 16381–16403 (2021).

73. Hu, W.-S., Liao, W.-Y., Chang, C.-H. & Chen, T.-S. Paracrine IGF-1 Activates SOD2 Expression and Regulates ROS/p53 Axis in the Treatment of Cardiac Damage in D-Galactose-Induced Aging Rats after Receiving Mesenchymal Stem Cells. *JCM* **11**, 4419 (2022).

74. El-Baz, F. K., Hussein, R. A., Saleh, D. O. & Abdel Jaleel, G. A. R. Zeaxanthin Isolated from Dunaliella salina Microalgae Ameliorates Age Associated Cardiac Dysfunction in Rats through Stimulation of Retinoid Receptors. *Marine Drugs* **17**, 290 (2019).

75. Ma, W. *et al*. Antioxidant Effect of Polygonatum sibiricum Polysaccharides in D-Galactose-Induced Heart Aging Mice. *BioMed Research International* **2021**, 1–8 (2021).

76. Cebe, T. *et al*. A comprehensive study of myocardial redox homeostasis in naturally and mimetically aged rats. *AGE* **36**, 9728 (2014).

77. Chang, Y.-M. *et al.* Adipose derived mesenchymal stem cells along with Alpinia oxyphylla extract alleviate mitochondria-mediated cardiac apoptosis in aging models and cardiac function in aging rats. *Journal of Ethnopharmacology* **264**, 113297 (2021).

78. Bo-Htay, C. *et al.* Aging induced by D-galactose aggravates cardiac dysfunction via exacerbating mitochondrial dysfunction in obese insulin-resistant rats. *GeroScience* **42**, 233–249 (2020).

79. Feng, W. *et al.* Alginate oligosaccharide alleviates D-galactose-induced cardiac ageing via regulating myocardial mitochondria function and integrity in mice. *J Cellular Molecular Medi* **25**, 7157–7168 (2021).

80. Guo, X.-H., Li, Y.-H., Zhao, Y.-S., Zhai, Y.-Z. & Zhang, L.-C. Anti-aging effects of melatonin on the myocardial mitochondria of rats and associated mechanisms. *Molecular Medicine Reports* **15**, 403–410 (2017).

81. Chang, Y.-M. *et al.* Anti-Apoptotic and Pro-Survival Effect of Alpinate Oxyphyllae Fructus (AOF) in a d-Galactose-Induced Aging Heart. *IJMS* **17**, 466 (2016).

82. Ge, Q. *et al.* Antioxidant activity of Lactobacillus plantarum NJAU-01 in an animal model of aging. *BMC Microbiol* **21**, 182 (2021).

83. Li, H. *et al.* Antioxidant, Anti-Aging and Organ Protective Effects of Total Saponins from Aralia taibaiensis. *DDDT* **Volume 15**, 4025–4042 (2021).

84. Charrière, N., Loonam, C., Montani, J.-P., Dulloo, A. G. & Grasser, E. K. Cardiovascular responses to sugary drinks in humans: galactose presents milder cardiac effects than glucose or fructose. *Eur J Nutr* **56**, 2105–2113 (2017).

85. Strother, R. M., Thomas, T. G., Otsyula, M., Sanders, R. A. & Iii, J. B. W. Characterization of Oxidative Stress in Various Tissues of Diabetic and Galactose-fed Rats. *Journal of Diabetes Research* **2**, 211–216 (2001).

86. Zhu, K. *et al.* Effect of insect tea on D-galactose-induced oxidation in mice and its mechanisms. *Food Science & Nutrition* **7**, 4105–4115 (2019).

87. Xue, Q., Aliabadi, H. & Hallfrisch, J. Effects of dietary galactose and fructose on rats fed diets marginal or adequate in copper for 9–21 months. *Nutrition Research* **21**, 1078–1087 (2001).

88. Chen, W.-K. *et al.* Exercise training augments Sirt1-signaling and attenuates cardiac inflammation in D-galactose induced-aging rats. *Aging* **10**, 4166–4174 (2018).

89. Lay, I.-S. *et al.* Exercise training restores IGFIR survival signaling in d-galactose induced-aging rats to suppress cardiac apoptosis. *Journal of Advanced Research* **28**, 35–41 (2021).

90. Yager, C., Ning, C., Reynolds, R., Leslie, N. & Segal, S. Galactitol and galactonate accumulation in heart and skeletal muscle of mice with deficiency of galactose-1-phosphate uridyltransferase. *Molecular Genetics and Metabolism* **81**, 105–111 (2004).

91. Zhang, H. *et al.* Hydrogen Sulfide Restored the Diurnal Variation in Cardiac Function of Aging Mice. *Oxidative Medicine and Cellular Longevity* **2021**, 1–10 (2021).

92. Park, D. J. *et al.* Induced Short-Term Hearing Loss due to Stimulation of Age-Related Factors by Intermittent Hypoxia, High-Fat Diet, and Galactose Injection. *IJMS* **21**, 7068 (2020).

93. Qian, Y. *et al.* Lactobacillus plantarum CQPC11 Isolated from Sichuan Pickled Cabbages Antagonizes d-galactose-Induced Oxidation and Aging in Mice. *Molecules* **23**, 3026 (2018).

94. Li, F. *et al.* *Lactobacillus plantarum* KSFY06 on D -galactose-induced oxidation and aging in Kunming mice. *Food Science & Nutrition* **8**, 379–389 (2020).

95. Cheng, J. *et al.* Mangiferin ameliorates cardiac fibrosis in D-galactose-induced aging rats by inhibiting TGF-β/p38/MK2 signaling pathway. *Korean J Physiol Pharmacol* **25**, 131–137 (2021).

96. Bei, Y. *et al.* miR-21 suppression prevents cardiac alterations induced by d-galactose and doxorubicin. *Journal of Molecular and Cellular Cardiology* **115**, 130–141 (2018).

97. Otsyula, M., King, M. S., Ketcham, T. G., Sanders, R. A. & Watkins, J. B. Oxidative Stress in Rats After 60 Days of Hypergalactosemia or Hyperglycemia. *Int J Toxicol* **22**, 423–427 (2003).

98. Chen, J. *et al.* Oxidative stress induces different tissue dependent effects on Mutyh-deficient mice. *Free Radical Biology and Medicine* **143**, 482–493 (2019).

99. Yi, R. *et al.* Preventive effect of insect tea primary leaf (*Malus sieboldii* (Regal) Rehd.) extract on D-galactose-induced oxidative damage in mice. *Food Science & Nutrition* **8**, 5160–5171 (2020).

100. Liu, B. *et al.* Protective Effect of Molecular Hydrogen Following Different Routes of Administration on D-Galactose-Induced Aging Mice. *JIR* **Volume 14**, 5541–5550 (2021).

101. Dehghani, A., Hafizibarjin, Z., Najjari, R., Kaseb, F. & Safari, F. Resveratrol and 1,25-dihydroxyvitamin D co-administration protects the heart against d-galactose-induced aging in rats: evaluation of serum and cardiac levels of klotho. *Aging Clin Exp Res* **31**, 1195–1205 (2019).

102. Musick, W. D. L. & Wells, W. W. Studies on galactose metabolism in heart and brain: The identification of d-galactose 6-phosphate in brains of galactose-intoxicated chicks and rat hearts perfused with galactose. *Archives of Biochemistry and Biophysics* **165**, 217–228 (1974).

103. Wang, L. *et al*. Tetrahydroberberrubine retards heart aging in mice by promoting PHB2-mediated mitophagy. *Acta Pharmacol Sin* **44**, 332–344 (2023).

104. Quan-Ma, R. & Wells, W. W. The distribution of galactitol in tissues of rats fed galactose. *Biochemical and Biophysical Research Communications* **20**, 486–490 (1965).

105. Guo, H. *et al*. The preventive effect of Apocynum□venetum polyphenols on D-galactose-induced oxidative stress in mice. *Exp Ther Med* (2019) doi:10.3892/etm.2019.8261.

106. El-Far, A. H. *et al*. Thymoquinone and Curcumin Defeat Aging-Associated Oxidative Alterations Induced by D-Galactose in Rats' Brain and Heart. *IJMS* **22**, 6839 (2021).

107. Mehdizadeh, M. *et al*. The role of cellular senescence in profibrillatory atrial remodelling associated with cardiac pathology. *Cardiovascular Research* **120**, 506–518 (2024).

108. Cardoso, A., Magano, S., Marrana, F. & Andrade, J. P. D -Galactose High-Dose Administration Failed to Induce Accelerated Aging Changes in Neurogenesis, Anxiety, and Spatial Memory on Young Male Wistar Rats. *Rejuvenation Research* **18**, 497–507 (2015).

109. Sengupta, P. The Laboratory Rat: Relating Its Age With Human's. *Int J Prev Med* **4**, 624–630 (2013).

110. Salkovic-Petrisic, M. *et al*. Long-term oral galactose treatment prevents cognitive deficits in male Wistar rats treated intracerebroventricularly with streptozotocin. *Neuropharmacology* **77**, 68–80 (2014).

111. Knezovic, A. *et al*. Glucagon-like peptide-1 mediates effects of oral galactose in streptozotocin-induced rat model of sporadic Alzheimer's disease. *Neuropharmacology* **135**, 48–62 (2018).

112. Chogtu, B. *et al*. Evaluation of Acute and Chronic Effects of D-Galactose on Memory and Learning in Wistar Rats. *Clin Psychopharmacol Neurosci* **16**, 153–160 (2018).

113. Homolak, J. *et al.* Is Galactose a Hormetic Sugar? An Exploratory Study of the Rat Hippocampal Redox Regulatory Network. *Molecular Nutrition Food Res* **65**, 2100400 (2021).

114. Homolak, J. *et al.* The Effect of Acute Oral Galactose Administration on the Redox System of the Rat Small Intestine. *Antioxidants* **11**, 37 (2021).

115. Sadigh-Eteghad, S. *et al.* D-galactose-induced brain ageing model: A systematic review and meta-analysis on cognitive outcomes and oxidative stress indices. *PLoS ONE* **12**, e0184122 (2017).

116. Homolak, J. *et al.* Separating science from science fiction: A non-existent enzyme is a primary driver of pathophysiological processes in galactose-induced rodent models of aging. (2020) doi:10.13140/RG.2.2.31233.89449/1.

6 SUPPLEMENTAL FIGURES

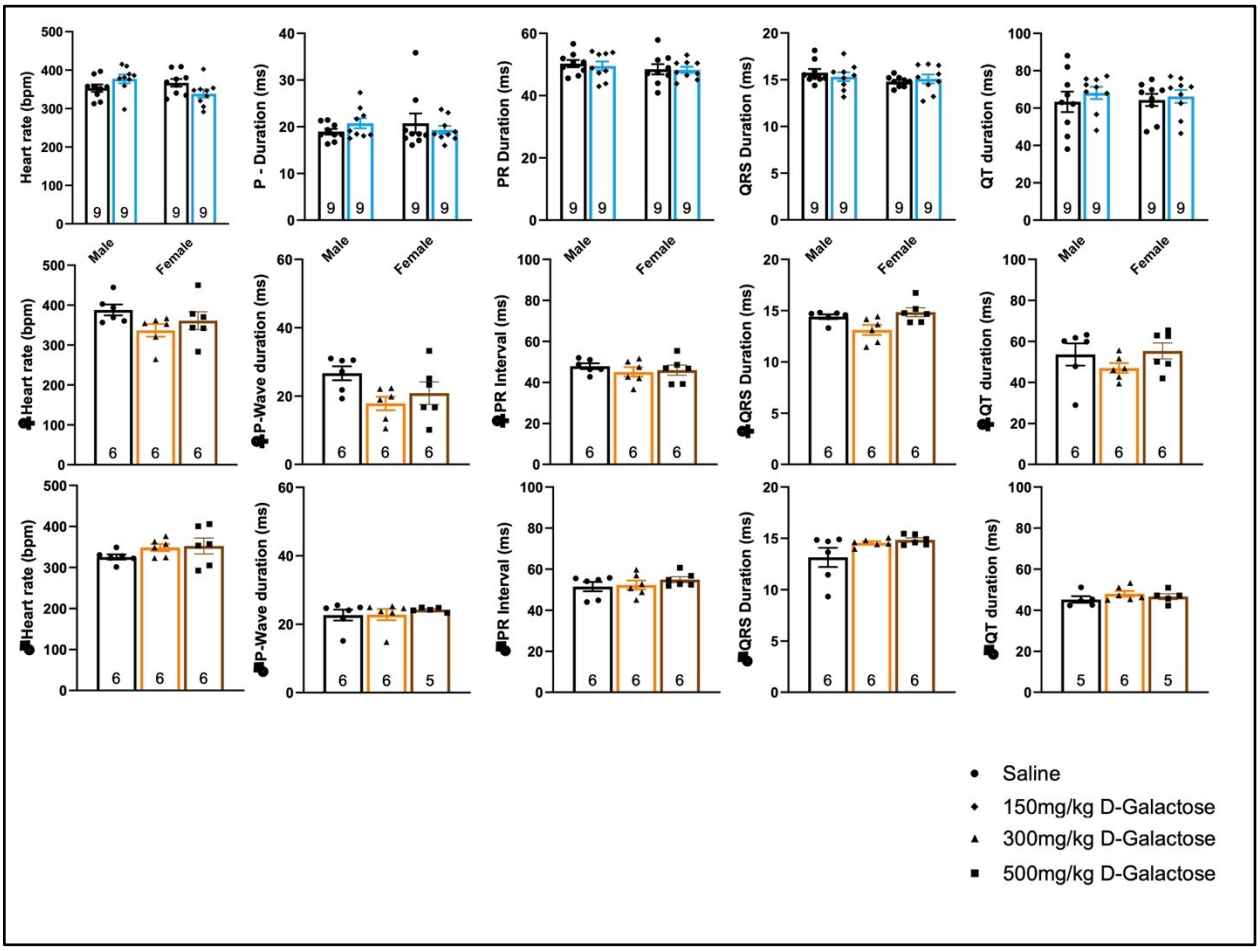

Figure S 1. ECG parameter changes by treatment. *Echocardiographic heartbeat parameters measured over all groups. (N=5-9) Statistical analysis: Low dose groups: two-way ANOVA, Sidak's multiple comparisons test, significance level P<0.05. Medium and high dose groups: one-way ANOVA, Holm-Sidak's multiple comparisons test, significance level P<0.05.*

S2. A

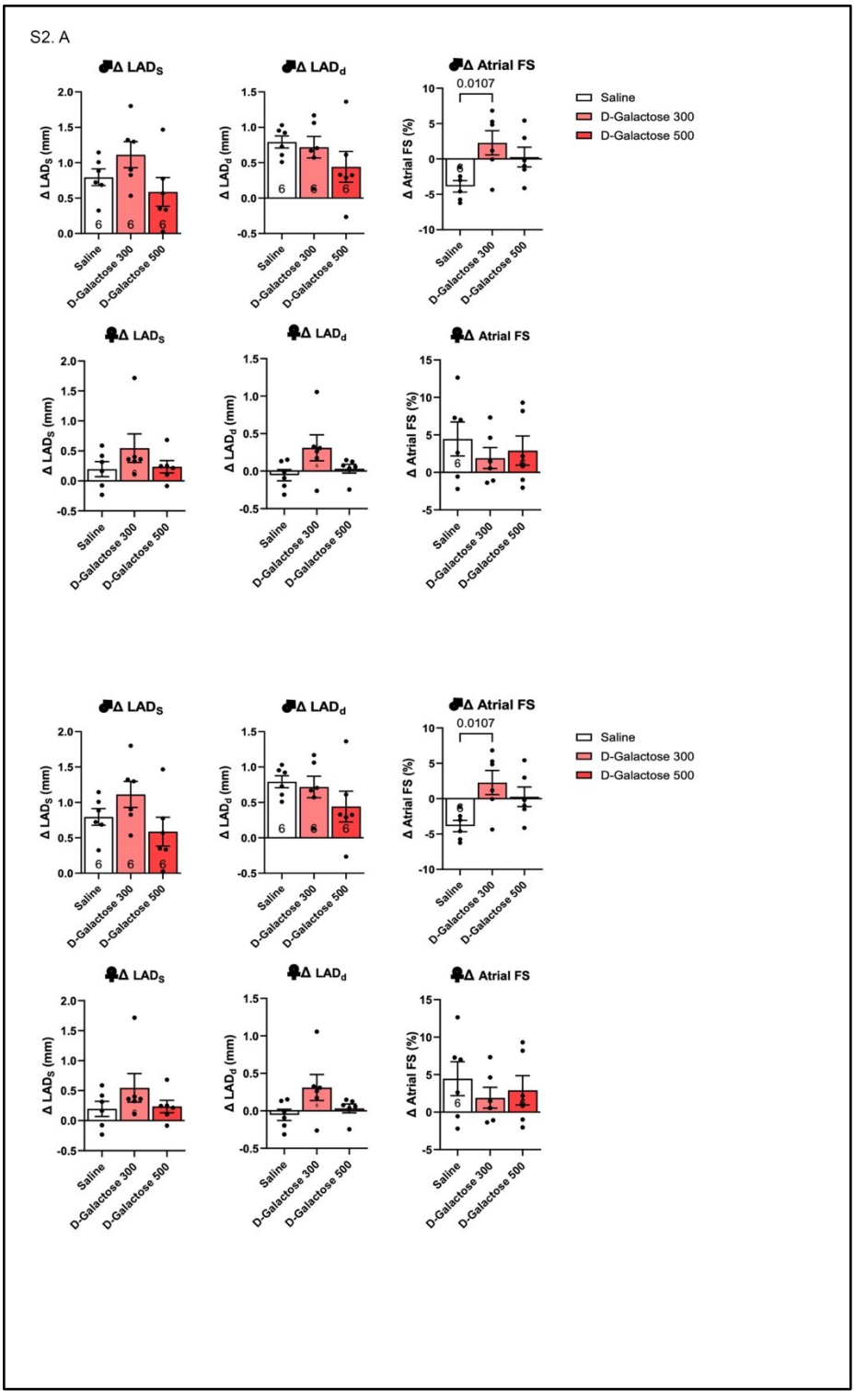
Δ LADS
Δ LADd
Δ Atrial FS
0.0107
Saline
D-Galactose 300
D-Galactose 500
Δ LADS (mm)
Δ LADd (mm)
Δ Atrial FS (%)

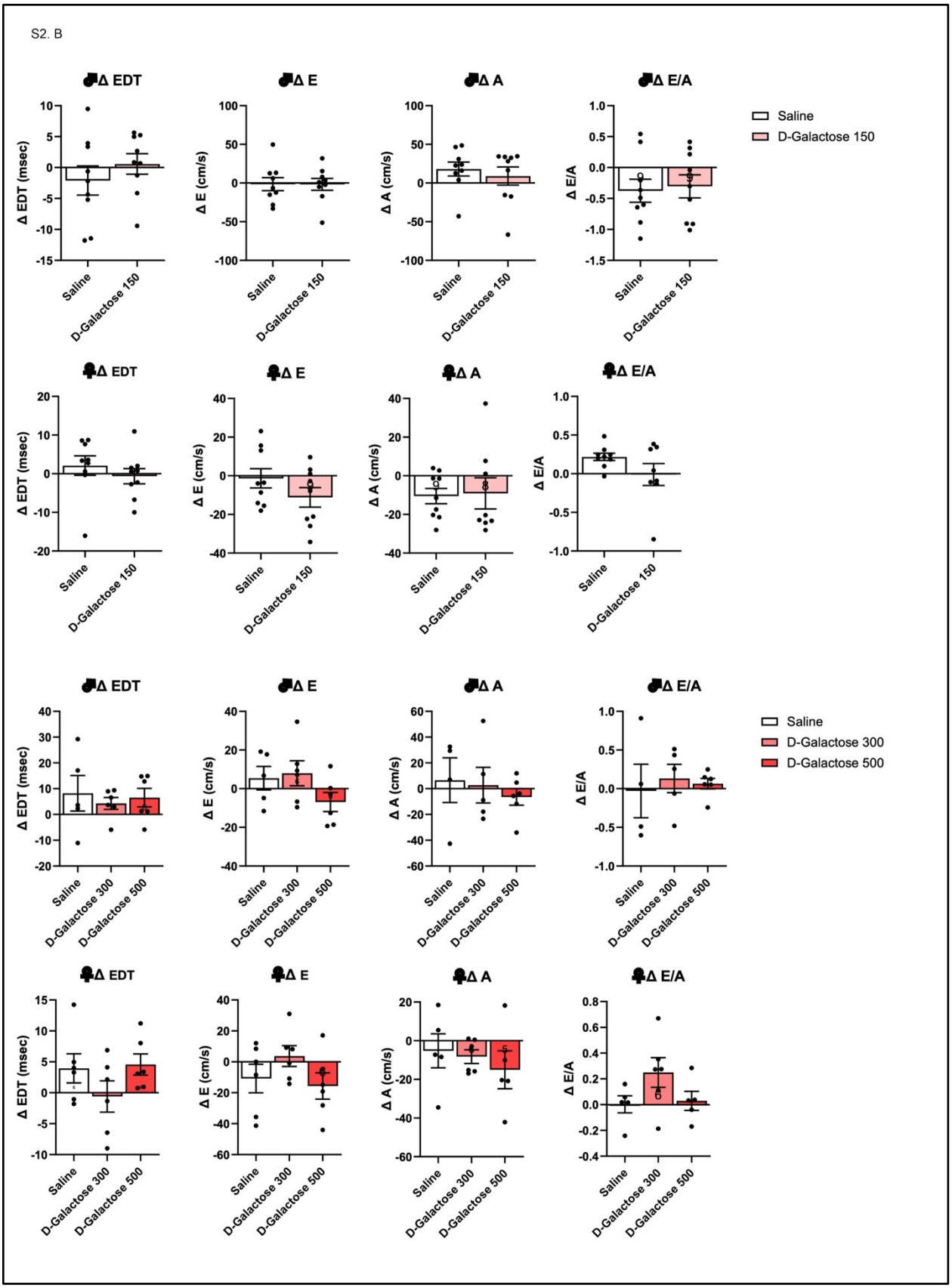
S2. B
♂Δ EDT
♂Δ E
♂Δ A
♂Δ E/A
♀Δ EDT
♀Δ E
♀Δ A
♀Δ E/A
Δ EDT (msec)
Δ E (cm/s)
Δ A (cm/s)
Δ E/A
Saline
D-Galactose 150
D-Galactose 300
D-Galactose 500

S2. C

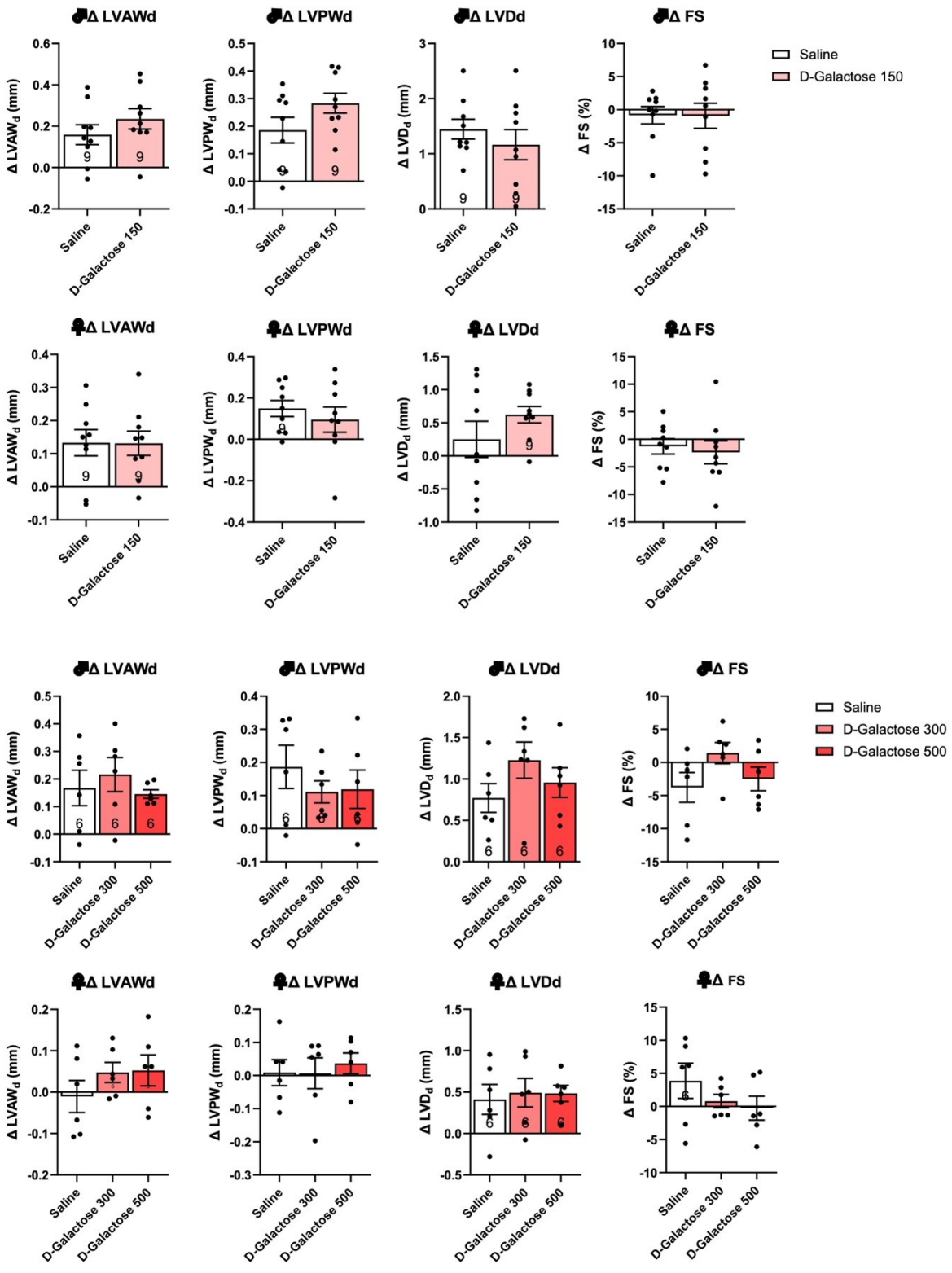
♂Δ LVAWd
♂Δ LVPWd
♂Δ LVDd
♂Δ FS
♀Δ LVAWd
♀Δ LVPWd
♀Δ LVDd
♀Δ FS
Δ LVAWd (mm)
Δ LVPWd (mm)
Δ LVDd (mm)
Δ FS (%)
Saline
D-Galactose 150
D-Galactose 300
D-Galactose 500

Figure S 2. Echocardiographic data of D-galactose treated, and vehicle treated rats. A) *Changes in LA dimensional parameters over all groups: LADs - left atrial dimension at end of systole; LADd - left atrial dimension at end of diastole; Atrial FS: overall atrial fractional shortening.* ***B)*** *Changes in left ventricular diastolic functional parameters over all groups: EDT: early filling deceleration time; A: trans mitral flow atrial filling; E: trans mitral flow early filling.* ***C)*** *left ventricular systolic functional and structural parameter changes over all groups: LVAWd: left ventricular anterior wall thickness at end of diastole; LVPWd: left ventricular posterior wall thickness at end of diastole. LVDd: left ventricle dimension at end of diastole; FS%: Left ventricular fractional shortening. Statistical analysis: Low dose group: unpaired t-test, significance level P<0.05. Medium and High dose groups: one-way ANOVA ; Dunnett's multiple comparisons test, significance level P<0.05.*

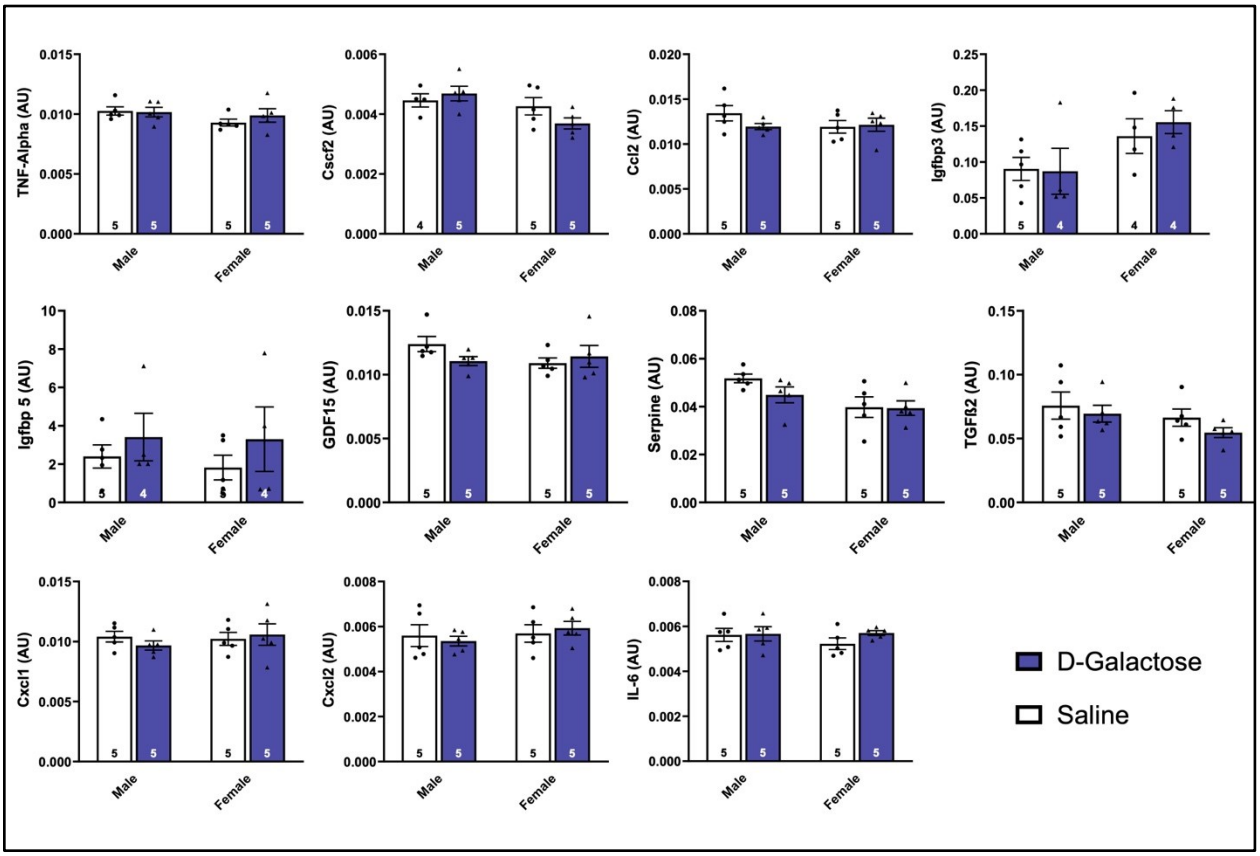

Figure S 3. mRNA expression of genes associated with cell-survival and apoptosis, inflammation, and extracellular matrix remodeling in low dose regimen rats. *Normalized to the geometric mean of the threshold cycle value of three housekeeping genes: B2m, Gapdh, and Hprt. (statistical analysis: two-way ANOVA ; Tukey's multiple comparison test, significance level P<0.05)*

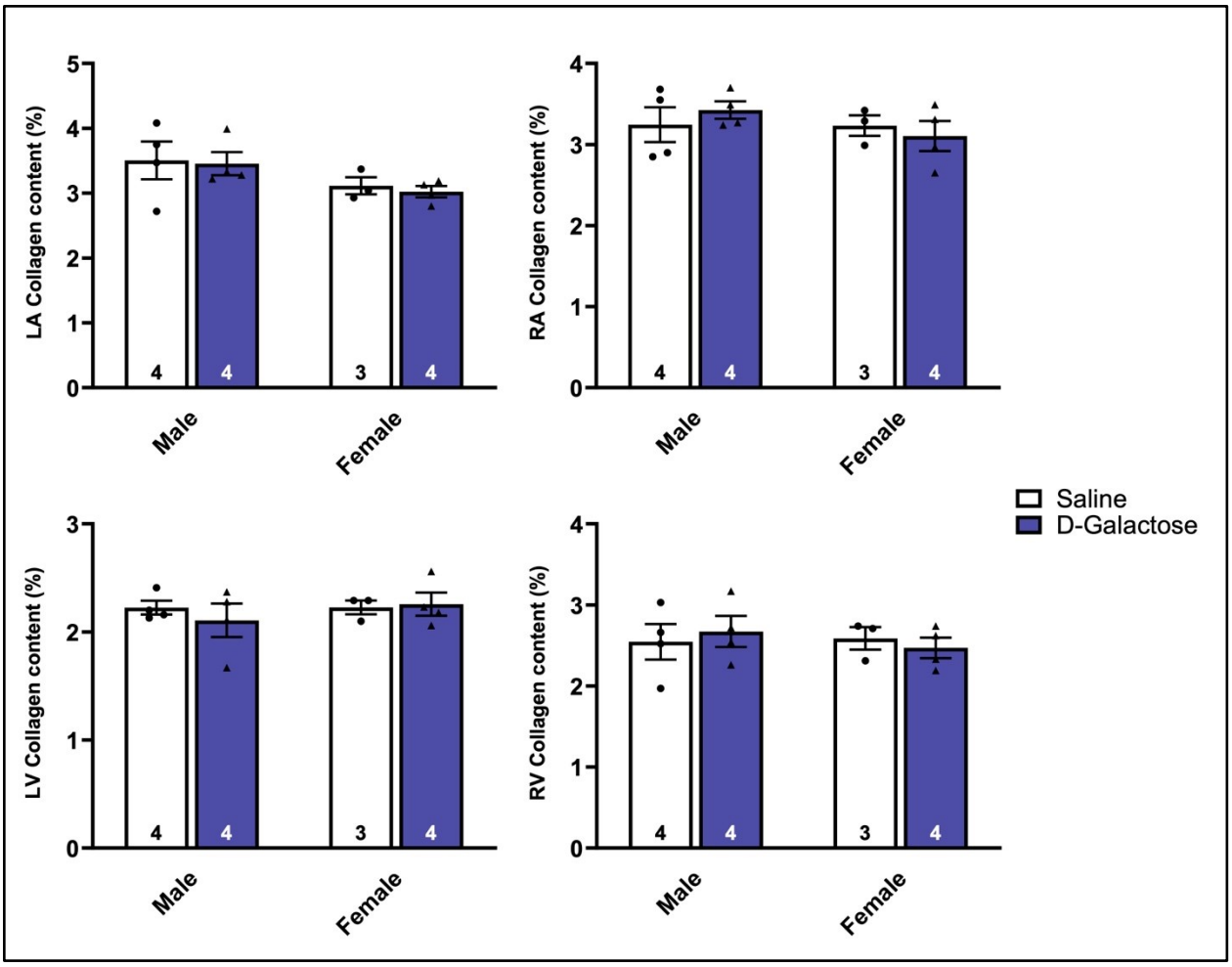

Figure S 4. Fibrosis quantification by percentage of tissue area for whole heart in low dose regimen rats. Images quantified by quadrant. *Analysis of each quadrant stained with Masson's Trichrome stain. Graph displays mean ± SEM fibrosis as a percentage of cross-sectional area of tissue. Each point represents an individual animal (N=3-4) (statistical analysis: two-way ANOVA ; Bonferroni multiple comparisons test, significance level p<0.05)*

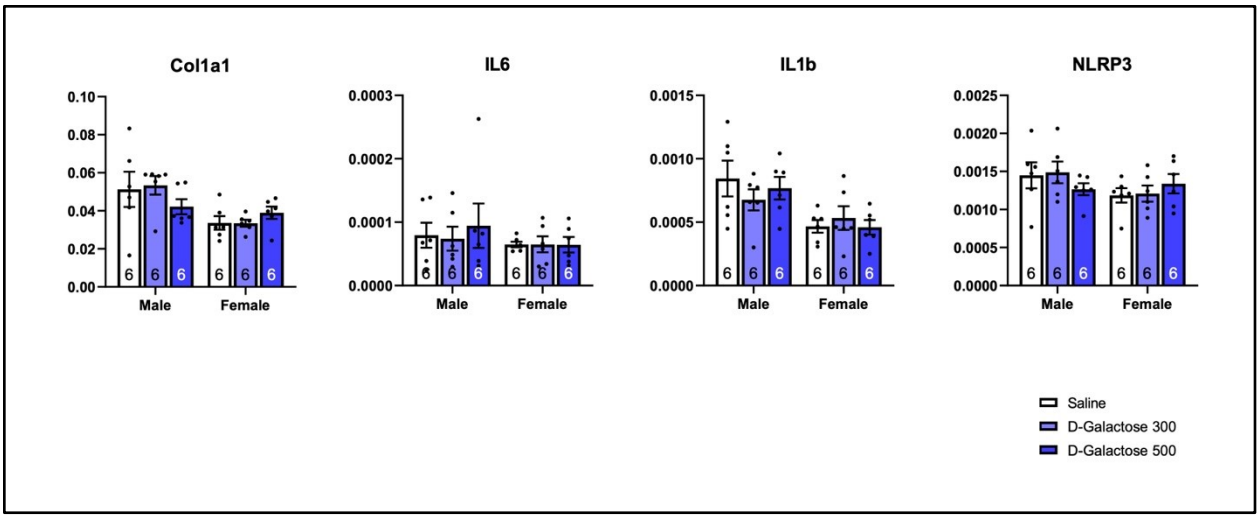

Figure S 5. mRNA expression of genes associated with inflammation, and fibrosis in medium and high dose regimen rats. *Normalized to the geometric mean of the threshold cycle value of three housekeeping genes: B2m, Gapdh, and Hprt. (statistical analysis: two-way ANOVA ; Dunnett's multiple comparison test, significance level P<0.05)*